

# Angular profiles of molecular beams from effusive tube sources: I. Experiment

F Rugamas<sup>†</sup>, D Roundy<sup>‡</sup>, G Mikaelian<sup>†</sup>, G Vitug<sup>†</sup>, M Rudner<sup>§||</sup>,  
J Shih<sup>§||</sup>, D Smith<sup>†</sup>, J Segura<sup>¶</sup> and M A Khakoo<sup>†</sup>

<sup>†</sup> Physics Department, California State University, Fullerton, CA 92834, USA

<sup>‡</sup> Department of Physics, University of California, Berkeley, CA 94720, USA

<sup>§</sup> Troy High School, Dorothy Lane, Fullerton, CA 92831, USA

<sup>¶</sup> Department of Mechanical Engineering, Stanford University, Stanford, CA 94305, USA

Received 31 March 2000, in final form and accepted for publication 14 July 2000

**Abstract.** New measurements of the angular distributions of effusive gas beams emanating from two collimating tube sources are presented. These sources are a single tube of aspect ratio 25 and a multi-capillary array of aspect ratio 100. The data were collected for a wide variety of gases (He, Ne, Ar, Kr, Xe, H<sub>2</sub>, N<sub>2</sub>, CO<sub>2</sub> and C<sub>2</sub>H<sub>2</sub>) over a broad range of driving pressures. The profiles were obtained by rotating the ionization gauge gas detector about the centre of the exit of the tube. The data were acquired as a function of the gas flow rate and pressure in the source line. Comparisons of the present measurements with other experimental work and models are made.

**Keywords:** free molecular flows, molecular beams

## 1. Introduction

There have been several efforts to characterize the profiles of collimated molecular beams emanating from effusive tube sources. These investigations have been motivated by applications of gas beams in molecular beam epitaxy, i.e. controlling such distributions with skimmers/focusing arrays with applications for UHV technology and measurement of collision cross-sections in beam–beam experiments using the popular ‘relative flow’ method. In our particular case, knowledge of molecular beam profiles is especially important when they are used in quantitative measurements of cross-sections, e.g. as discussed by Ramsey (1990) and Brinkmann and Trajmar (1981). In the widely employed method of relative flow (Srivastava *et al* 1975, Trajmar and Register 1984), the collision (absorption) cross-section of a standard gas can be compared with that of an unknown gas provided that the collision geometry of the overlap of the scattering beams and the fluences are known accurately. This comparison is facilitated by operating the standard and the unknown gas beams so that their profiles are the same. This is achieved by running the two gases so that the mean free-paths of the two gases in the reservoir behind the collimating structure (used to generate the beam) are the same. When the profiles of the two gases are the same, the signals in a scattering or absorption experiment,  $I_x$  and  $I_c$  (where  $x$  and

$c$  represent the unknown and calibration gases), are related to the cross-sections by the formula

$$\sigma_x = \frac{\sigma_c I_x \dot{N}_c}{I_c \dot{N}_x} \left( \frac{M_c}{M_x} \right)^{1/2} \quad (1)$$

where  $\sigma$  is the (respective) collision cross-section and  $\dot{N}$  is the flow rate of the gas of relative molecular mass  $M$ . Equation (1) assumes that the two gases are at the same temperature. Despite the simplicity of its application, there are significant differences in measured electron–gas scattering cross-sections among experiments which have used the relative flow technique in the past (see e.g. Trajmar *et al* (1983)). Buckman *et al* (1993) recently suggested that the mean free-path condition applied only at low reservoir pressures, i.e. at pressures not significantly higher than those of free-molecular flow. This observation is in contrast to the work of Olander and co-workers (see e.g. Olander and Kruger (1970)), who conclude that the mean free-path condition should be valid over a higher pressure range extending into the region where atomic/molecular collisions in the collimating structure became significant. Our motivations for this work are the following.

- (i) To investigate the range of validity of the mean free-path condition and to see where its breakdown takes place.
- (ii) To obtain data in which both the gas flow rate and the reservoir pressure are recorded. Experimentally, flow rates can be accurately measured, whereas source

|| Present address: California Institute of Technology, Pasadena, CA 91126, USA.

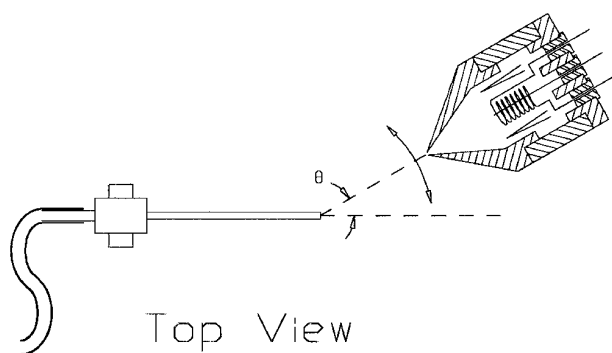


**Figure 1.** A schematic drawing of the ionization gauge neutral beam detector, showing the placement of the dual filaments, grid coil and collector (central wire).

reservoir pressures cannot be easily measured, unless the manometer is placed immediately before the collimating structure. Thus the flow rate serves as a good monitor of the source conditions and is free of conductance effects in the plumbing that supplies gas to the collimating tube.

- (iii) To observe the variation of the angular profile of the gas as a function of the distance from the exit of the tube.

In this series of papers, part I will be concerned with our measurements of beam profiles as a function of the flow rate and source reservoir pressure. Part II will be concerned with our Monte Carlo modelling of these profiles with respect to gas pressures and flow rates and part III will be concerned with the application of the information in parts I and II towards an understanding of the relative flow method.

Two experimental geometries are typically employed to measure gas beam profiles. (A) The profile may be obtained by an angular scan of the gas beam as a function of the angle  $\theta$  (see figure 1) with the detector rotation centred about the entrance of the gas forming tube. (B) The profile may be obtained by spatially scanning the intensity of the gas beam along a linear path intersecting the gas forming tube axis but perpendicular to it.

In method A, the solid angle  $\Delta\Omega_A$  subtended by the detector at the source remains constant. This can be related to the detector solid angle  $\Delta\Omega_B$  in method B, which changes with  $\theta$ , according to the relation

$$\Delta\Omega_B(\theta) = \Delta\Omega_A \cos^3(\theta). \quad (2)$$

There are two distinct advantages of method A over method B. First, in method A, a true profile,  $I(\theta)$ , of the gas beam is obtained since the signal is proportional to  $I(\theta)\Delta\Omega_A$ , whereas method B yields a signal proportional to  $I(\theta)\Delta\Omega_B = I(\theta)\Delta\Omega_A \cos^3(\theta)$ . This means that large-angle structure in  $I(\theta)$  is not fully observable in method B. Additionally,  $|\theta| > 90^\circ$  can be reached with method A, to immediately obtain the true background contribution of gas in the vacuum tank. To determine the background in method B, a somewhat indirect method, e.g. of diverting the gas flow through the source tube elsewhere into the vacuum tank, must be employed.

Some of the past experimental investigations of this type were performed by Giordmaine and Wang (1960), Hanes (1960), Jones *et al* (1969), Steinruck and Redulic

(1986), Adamson and McGilp (1986, 1988), Adamson *et al* (1988) and, more recently, Buckman *et al* (1993). Most of these measurements have used large separations between the source and the detector (40 cm or greater); however, the most recent of these, by Jones *et al* (1969), Adamson and McGilp (1988), Adamson *et al* (1988) and Buckman *et al* (1993), obtained distributions for single capillary and multi-capillary arrays at separations of as little as 1.5 mm from the source tube. A summary of these experiments is given in table 1. Buckman *et al* used method B to measure spatial full widths at half maxima (FWHMs) of the gas beam profiles for various gases as a function of the mean free-path ( $\lambda$ ) and minimum detector–source separation. They found, significant differences among the FWHMs for the six gases considered for the same  $\lambda$  and that this difference increased as the minimum detector–source separation was increased from 1.5 to 4.5 mm. In particular, they found marked differences between He and the other gases used ( $H_2$  to Kr and  $N_2$ ). In their work they noted the smallest source–detector distance used and also took measurements over a wide range of source driving pressures,  $P_s$ . Adamson and McGilp (1986, 1988) (also using method B) focused on the comparison between experimental profiles and theoretical analytical profiles of Zugenmaier (1965), Jones *et al* (1969) and Clausing (1930). They found significant discrepancies at moderate pressures between the various theories and their experimental data. The situation improved as the pressure was reduced so that length Knudsen values ( $K_L = \lambda/L$ , where  $L$  is the tube length in the same units as  $\lambda$ ) of greater than 100 were reached. Adamson *et al* repeated these measurements over a more extended range and developed a Monte Carlo algorithm based on the analytical (approximation) work of Giordmaine and Wang (1960). They found that the simple Monte Carlo algorithm (which considered only specular collisions with the tube walls) was in excellent agreement with their data. It must be pointed out that, since this work was carried out at large  $K_L$  (low driving pressure), such gas beams are tenuous. Although such (tenuous) beams are excellent for molecular beam epitaxy, they are typically less intense than gas beams used in beam–beam collision studies. In most beam–beam collision studies typical Knudsen numbers range from  $K_L \approx 1$  to  $K_D \ll 1$  ( $K_D = \lambda/D$ , where  $D$  is the tube diameter in the same units). In the regime of  $K_L \approx 1$ , the mean free-path is comparable to the tube length and therefore inter-atomic/molecular collisions in the tube do not play any (major) role in the collimation of the beam. In the intermediate region of  $K_L \leq 1$  and  $K_D > 1$ , the regime is one of transition between free-molecular flow and viscous flow. Now inter-atomic/molecular collisions become significant, affecting both the profile and the dependence of the flow rate on the reservoir pressure. When  $K_D < 1$ , the mean free-path is shorter than the tube diameter and collisions take place throughout the entire length of the tube.

To investigate the operation of such tube sources, initial modelling work was done by Giordmaine and Wang (1960). This was followed by the works of Olander and Kruger (1970), Lucas (1973) and Murphy (1989). The condition for effusion of the gas requires that the number density drop linearly with distance, since the flow rate of gas,  $dN/dt$ ,

**Table 1.** A summary of existing measurements of effusive gas beam profiles from tubular collimating sources. Distances  $r$  for Hanes' (1960) measurements are not given, but are estimated to be  $>20$  mm from his figure. S, single tube; M, multi-capillary array.

Source	Method	Distance	Tube type
Giordmaine and Wang (1960)	A	40.5 cm	S
Hanes (1960)	A	Large	
Jones <i>et al</i> (1969)	A	50 mm	S, M
Steinruck and Redulic (1986)	A	100 mm	
Adamson and McGilp (1986, 1988)	B	12 mm	S
Adamson <i>et al</i> (1988)	B	12–15 mm	S
Buckman <i>et al</i> (1993)	B	1.5–4.5 mm	S, M

**Table 2.** A list of molecular diameters (with corresponding references) for pertinent gases used in this research. Units are  $10^{-8}$  cm. Source references are used for column headings.

Gas	Dushman (1949) viscosity	Guthrie (1963) viscosity	CRC (1969) viscosity	CRC (1969) Van der Waals	CRC (1969) conductivity	Roth (1987) viscosity	Trajmar and Register (1984) various	Present gas flow
H <sub>2</sub>	2.75	2.74	2.4	2.34	2.32		2.76	2.74
He	2.18	2.18	1.9	2.65	2.3		2.20	2.18
Ne	2.60	2.59					2.60	2.50
A	3.67	3.64	2.88	2.94	2.86		3.66	3.64
Xe	4.91			4.02	3.42			3.60
N <sub>2</sub>		3.75	3.15	3.15	3.53		3.78	3.75
C <sub>2</sub> H <sub>2</sub>						4.95		4.30
CO <sub>2</sub>	4.65	4.59	3.34	3.23	3.4		4.64	4.65

**Table 3.**  $a$  and  $\epsilon$  parameters obtained (with one standard deviation errors) from fits to  $dN/dt$  versus  $P$  for the tube source. The derived relative molecular diameters  $\delta_R$  (in units of  $10^{-8}$  cm) are normalized with respect to the  $\delta$  of He at  $2.18 \times 10^{-8}$  cm. See the text for details and definitions of parameters.

Gas	$M$	$\delta$	$a$	$\Delta a$	$\epsilon$	$\Delta \epsilon$	$\delta_R$	$\Delta \delta_R$
H <sub>2</sub>	2	2.74	20 616	1014	6.87	0.60	2.81	0.50
He	4	2.18	15 009	919	4.15	0.65	2.18	—
Ne	20.2	2.60	7297	365	5.50	0.99	2.51	0.60
C <sub>2</sub> H <sub>2</sub>	26	5.00	5699	253	24.28	1.71	5.28	0.90
N <sub>2</sub>	28	3.75	5602	360	13.86	1.31	3.99	0.73
Ar	39.9	3.64	4754	371	12.40	1.72	3.77	0.79
CO <sub>2</sub>	44	4.55	5073	369	17.42	2.20	4.47	0.90
Xe	131	4.91	2540	241	23.94	3.10	5.24	1.07

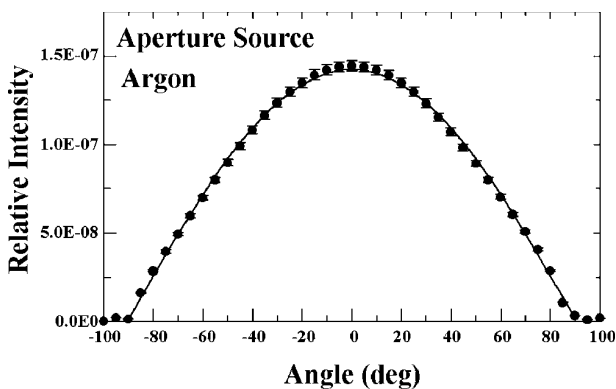


**Figure 2.** Observation of the angular gas beam profile of a 0.2 mm diameter 0.05 mm thick aperture and fitting of this with a  $\cos \theta$  dependence. See the text for a description.

is determined by the gradient of the number density as a function of distance,  $z$ , down the tube from the reservoir. Thus,

$$dN/dt = -KdN/dz. \quad (3)$$

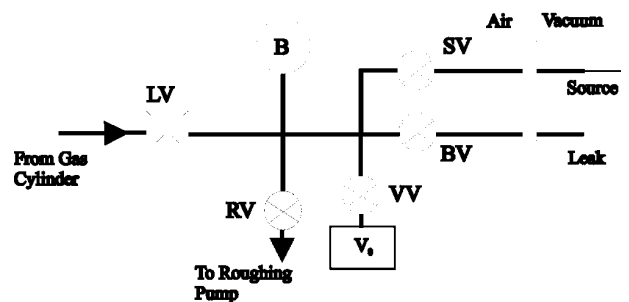


**Figure 3.** A schematic diagram of the arrangement of the gas beam handling system for the present experiments. See the text for a detailed description.

$K$  is a constant related to the cross-sectional area of the tube, gas temperature and mean velocity. The main problem in these models is the determination of the exit number density (Olander and Kruger 1970), which would allow  $dN/dz$  to be correctly determined. Various schemes have been used and are summarized in Adamson and McGilp (1988). Giordmaine and Wang (1960) considered the attenuation

**Table 4.** A summary of measurements for atomic gases using the tube source, with  $D = 0.08$  cm and  $L = 20$  cm. See the text for descriptions of parameters.

He				
$P$ (Torr)	$dN/dt$ ( $s^{-1}$ )	$\lambda$ (cm)	$\theta_{1/2}$ (deg)	$\theta_{1/2}^c$ (deg)
$5.49 \times 10^{-3}$	$7.79 \times 10^{+14}$	$2.68 \times 10^0$	$7.40 \times 10^0$	$6.88 \times 10^0$
$2.38 \times 10^{-2}$	$3.38 \times 10^{+15}$	$6.17 \times 10^{-1}$	$1.01 \times 10^{+1}$	$9.52 \times 10^0$
$3.24 \times 10^{-2}$	$5.04 \times 10^{+15}$	$4.54 \times 10^{-1}$	$1.15 \times 10^{+1}$	$1.07 \times 10^{+1}$
$4.47 \times 10^{-2}$	$6.98 \times 10^{+15}$	$3.29 \times 10^{-1}$	$1.28 \times 10^{+1}$	$1.19 \times 10^{+1}$
$5.69 \times 10^{-2}$	$9.97 \times 10^{+15}$	$2.59 \times 10^{-1}$	$1.45 \times 10^{+1}$	$1.31 \times 10^{+1}$
$6.59 \times 10^{-2}$	$1.20 \times 10^{+16}$	$2.23 \times 10^{-1}$	$1.59 \times 10^{+1}$	$1.39 \times 10^{+1}$
$1.12 \times 10^{-1}$	$2.36 \times 10^{+16}$	$1.32 \times 10^{-1}$	$2.02 \times 10^{+1}$	$1.65 \times 10^{+1}$
$2.08 \times 10^{-1}$	$5.78 \times 10^{+16}$	$7.08 \times 10^{-2}$	$2.75 \times 10^{+1}$	$2.08 \times 10^{+1}$
$2.50 \times 10^{-1}$	$7.53 \times 10^{+16}$	$5.89 \times 10^{-2}$	$2.93 \times 10^{+1}$	$2.19 \times 10^{+1}$
$2.69 \times 10^{-1}$	$8.39 \times 10^{+16}$	$5.47 \times 10^{-2}$	$3.13 \times 10^{+1}$	$2.26 \times 10^{+1}$
$2.96 \times 10^{-1}$	$9.71 \times 10^{+16}$	$4.97 \times 10^{-2}$	$3.20 \times 10^{+1}$	$2.31 \times 10^{+1}$
$3.26 \times 10^{-1}$	$1.13 \times 10^{+17}$	$4.51 \times 10^{-2}$	$3.36 \times 10^{+1}$	$2.38 \times 10^{+1}$
$3.64 \times 10^{-1}$	$1.37 \times 10^{+17}$	$4.05 \times 10^{-2}$	$3.45 \times 10^{+1}$	$2.43 \times 10^{+1}$
$6.80 \times 10^{-1}$	$3.85 \times 10^{+17}$	$2.16 \times 10^{-2}$	$3.95 \times 10^{+1}$	$2.79 \times 10^{+1}$
$7.70 \times 10^{-1}$	$4.96 \times 10^{+17}$	$1.91 \times 10^{-2}$	$4.33 \times 10^{+1}$	$2.92 \times 10^{+1}$
$8.35 \times 10^{-1}$	$5.52 \times 10^{+17}$	$1.76 \times 10^{-2}$	$4.39 \times 10^{+1}$	$3.00 \times 10^{+1}$
$1.01 \times 10^0$	$7.84 \times 10^{+17}$	$1.46 \times 10^{-2}$	$4.50 \times 10^{+1}$	$3.18 \times 10^{+1}$
Ne				
$P$ (Torr)	$dN/dt$ ( $s^{-1}$ )	$\lambda$ (cm)	$\theta_{1/2}$ (deg)	$\theta_{1/2}^c$ (deg)
$1.27 \times 10^{-2}$	$1.01 \times 10^{+15}$	$8.17 \times 10^{-1}$	$1.01 \times 10^{+1}$	$9.60 \times 10^0$
$2.74 \times 10^{-2}$	$2.10 \times 10^{+15}$	$3.78 \times 10^{-1}$	$1.27 \times 10^{+1}$	$1.17 \times 10^{+1}$
$3.32 \times 10^{-2}$	$2.76 \times 10^{+15}$	$3.11 \times 10^{-1}$	$1.38 \times 10^{+1}$	$1.25 \times 10^{+1}$
$4.10 \times 10^{-2}$	$3.44 \times 10^{+15}$	$2.53 \times 10^{-1}$	$1.53 \times 10^{+1}$	$1.36 \times 10^{+1}$
$4.16 \times 10^{-2}$	$3.53 \times 10^{+15}$	$2.49 \times 10^{-1}$	$1.52 \times 10^{+1}$	$1.36 \times 10^{+1}$
$5.08 \times 10^{-2}$	$4.33 \times 10^{+15}$	$2.04 \times 10^{-1}$	$1.69 \times 10^{+1}$	$1.46 \times 10^{+1}$
$6.62 \times 10^{-2}$	$5.99 \times 10^{+15}$	$1.56 \times 10^{-1}$	$1.87 \times 10^{+1}$	$1.59 \times 10^{+1}$
$9.61 \times 10^{-2}$	$1.04 \times 10^{+16}$	$1.08 \times 10^{-1}$	$2.29 \times 10^{+1}$	$1.82 \times 10^{+1}$
$1.17 \times 10^{-1}$	$1.34 \times 10^{+16}$	$8.84 \times 10^{-2}$	$2.54 \times 10^{+1}$	$1.97 \times 10^{+1}$
$1.49 \times 10^{-1}$	$1.92 \times 10^{+16}$	$6.97 \times 10^{-2}$	$2.86 \times 10^{+1}$	$2.15 \times 10^{+1}$
$2.26 \times 10^{-1}$	$3.68 \times 10^{+16}$	$4.58 \times 10^{-2}$	$3.35 \times 10^{+1}$	$2.40 \times 10^{+1}$
$2.46 \times 10^{-1}$	$4.27 \times 10^{+16}$	$4.21 \times 10^{-2}$	$3.44 \times 10^{+1}$	$2.45 \times 10^{+1}$
$2.65 \times 10^{-1}$	$4.66 \times 10^{+16}$	$3.90 \times 10^{-2}$	$3.51 \times 10^{+1}$	$2.49 \times 10^{+1}$
$2.69 \times 10^{-1}$	$4.74 \times 10^{+16}$	$3.85 \times 10^{-2}$	$3.54 \times 10^{+1}$	$2.50 \times 10^{+1}$
$3.16 \times 10^{-1}$	$6.37 \times 10^{+16}$	$3.27 \times 10^{-2}$	$3.78 \times 10^{+1}$	$2.59 \times 10^{+1}$
$5.58 \times 10^{-1}$	$1.65 \times 10^{+17}$	$1.85 \times 10^{-2}$	$4.25 \times 10^{+1}$	$2.87 \times 10^{+1}$
$6.52 \times 10^{-1}$	$2.20 \times 10^{+17}$	$1.59 \times 10^{-2}$	$4.30 \times 10^{+1}$	$3.02 \times 10^{+1}$
$7.33 \times 10^{-1}$	$2.68 \times 10^{+17}$	$1.41 \times 10^{-2}$	$4.54 \times 10^{+1}$	$3.12 \times 10^{+1}$

of the forward moving gas in the tube in terms of hard-sphere scattering. However, their assumption of a zero density at the exit means that they cannot derive realistic values of the flow rate from their calculations, although their calculations should yield reasonable gas beam profiles for low pressures appertaining to  $K_L \geq 1$ . Theoretical profiles, e.g. of Giordmaine and Wang (1960) and others, are based on hard-sphere scattering (see Adamson and McGilp (1988)). To provide more realistic profiles, soft-sphere scattering needs to be included. Additionally, the assumption of specular reflection at the tube walls is *ad hoc*. This has been recently pointed out and reviewed by Thomson and Owens (1975). They stress that a combination of diffuse and specular reflection of the gas from the walls of the tube is needed in theoretical models of the flow of gas beams down tubes. However, Thomson and Owens restrict their analysis to flow rates only; they do not consider angular distributions of gas beam profiles. One can expect the various atom/molecule-tube reflection mechanisms to strongly affect the gas beam

profile, especially in the free-molecular flow regime,  $K_L \geq 1$ . In the regime of  $K_L \leq 1$ , the profile will be increasingly dominated by inter-atomic/molecular collisions.

In the present work, where we have used the configuration of method A, our motivation for studying gas beam profiles concerns the application of the relative flow method (Srivastava *et al* 1975) for collision cross-section measurements in beam-beam experiments. The reasons for this choice have been discussed previously. In this paper we present the results and analysis of our experimental work and its implications for the relative flow method.

## 2. Experimental details

The experimental data were taken in two vacuum tanks over a period of two years. Both vacuum tanks were evacuated by clean diffusion pumps with Santovac 10 oil and could be pumped down to approximately  $10^{-7}$  Torr. Figure 1 shows schematically the arrangement of the experiment.

Table 4. (Continued)

Ar				
$P$ (Torr)	$dN/dt$ ( $s^{-1}$ )	$\lambda$ (cm)	$\theta_{1/2}$ (deg)	$\theta_{1/2}^c$ (deg)
$6.00 \times 10^{-4}$	$1.44 \times 10^{+13}$	$8.80 \times 10^0$	$7.40 \times 10^0$	$7.10 \times 10^0$
$3.69 \times 10^{-3}$	$2.11 \times 10^{+14}$	$1.43 \times 10^0$	$9.00 \times 10^0$	$8.70 \times 10^0$
$9.09 \times 10^{-3}$	$4.12 \times 10^{+14}$	$5.81 \times 10^{-1}$	$1.02 \times 10^{+1}$	$9.50 \times 10^0$
$1.35 \times 10^{-2}$	$6.59 \times 10^{+14}$	$3.92 \times 10^{-1}$	$1.29 \times 10^{+1}$	$1.20 \times 10^{+1}$
$1.41 \times 10^{-2}$	$8.15 \times 10^{+14}$	$3.73 \times 10^{-1}$	$1.38 \times 10^{+1}$	$1.26 \times 10^{+1}$
$1.72 \times 10^{-2}$	$8.87 \times 10^{+14}$	$3.08 \times 10^{-1}$	$1.43 \times 10^{+1}$	$1.31 \times 10^{+1}$
$2.19 \times 10^{-2}$	$1.31 \times 10^{+15}$	$2.41 \times 10^{-1}$	$1.65 \times 10^{+1}$	$1.46 \times 10^{+1}$
$4.03 \times 10^{-2}$	$2.72 \times 10^{+15}$	$1.31 \times 10^{-1}$	$2.12 \times 10^{+1}$	$1.77 \times 10^{+1}$
$5.86 \times 10^{-2}$	$4.64 \times 10^{+15}$	$9.01 \times 10^{-2}$	$2.59 \times 10^{+1}$	$2.01 \times 10^{+1}$
$6.67 \times 10^{-2}$	$5.84 \times 10^{+15}$	$7.91 \times 10^{-2}$	$2.79 \times 10^{+1}$	$2.13 \times 10^{+1}$
$8.59 \times 10^{-2}$	$8.38 \times 10^{+15}$	$6.15 \times 10^{-2}$	$3.11 \times 10^{+1}$	$2.29 \times 10^{+1}$
$9.16 \times 10^{-2}$	$9.11 \times 10^{+15}$	$5.77 \times 10^{-2}$	$3.10 \times 10^{+1}$	$2.31 \times 10^{+1}$
$1.15 \times 10^{-1}$	$1.37 \times 10^{+16}$	$4.58 \times 10^{-2}$	$3.47 \times 10^{+1}$	$2.46 \times 10^{+1}$
$1.65 \times 10^{-1}$	$2.34 \times 10^{+16}$	$3.20 \times 10^{-2}$	$3.70 \times 10^{+1}$	$2.62 \times 10^{+1}$
$1.92 \times 10^{-1}$	$3.10 \times 10^{+16}$	$2.75 \times 10^{-2}$	$3.88 \times 10^{+1}$	$2.70 \times 10^{+1}$
$2.28 \times 10^{-1}$	$4.15 \times 10^{+16}$	$2.32 \times 10^{-2}$	$4.08 \times 10^{+1}$	$2.75 \times 10^{+1}$
$2.78 \times 10^{-1}$	$5.76 \times 10^{+16}$	$1.90 \times 10^{-2}$	$4.22 \times 10^{+1}$	$2.88 \times 10^{+1}$
$3.07 \times 10^{-1}$	$6.75 \times 10^{+16}$	$1.72 \times 10^{-2}$	$4.41 \times 10^{+1}$	$2.98 \times 10^{+1}$
$3.31 \times 10^{-1}$	$7.95 \times 10^{+16}$	$1.59 \times 10^{-2}$	$4.41 \times 10^{+1}$	$2.99 \times 10^{+1}$
$3.64 \times 10^{-1}$	$9.26 \times 10^{+16}$	$1.45 \times 10^{-2}$	$4.52 \times 10^{+1}$	$3.01 \times 10^{+1}$
$3.82 \times 10^{-1}$	$1.01 \times 10^{+17}$	$1.38 \times 10^{-2}$	$4.60 \times 10^{+1}$	$3.15 \times 10^{+1}$
$4.89 \times 10^{-1}$	$1.58 \times 10^{+17}$	$1.08 \times 10^{-2}$	$4.87 \times 10^{+1}$	$3.25 \times 10^{+1}$
$6.21 \times 10^{-1}$	$2.51 \times 10^{+17}$	$8.49 \times 10^{-3}$	$5.05 \times 10^{+1}$	$3.27 \times 10^{+1}$
$8.70 \times 10^{-1}$	$4.51 \times 10^{+17}$	$6.07 \times 10^{-3}$	$5.35 \times 10^{+1}$	$3.44 \times 10^{+1}$
$9.88 \times 10^{-1}$	$5.81 \times 10^{+17}$	$5.34 \times 10^{-3}$	$5.52 \times 10^{+1}$	$3.60 \times 10^{+1}$
Xe				
$P$ (Torr)	$dN/dt$ ( $s^{-1}$ )	$\lambda$ (cm)	$\theta_{1/2}$ (deg)	$\theta_{1/2}^c$ (deg)
$1.39 \times 10^{-3}$	$4.06 \times 10^{+13}$	$2.09 \times 10^0$	$7.60 \times 10^0$	$7.35 \times 10^0$
$2.17 \times 10^{-3}$	$7.23 \times 10^{+13}$	$1.34 \times 10^0$	$9.70 \times 10^0$	$9.20 \times 10^0$
$5.50 \times 10^{-3}$	$1.77 \times 10^{+14}$	$5.27 \times 10^{-1}$	$1.16 \times 10^{+1}$	$1.08 \times 10^{+1}$
$5.72 \times 10^{-3}$	$1.89 \times 10^{+14}$	$5.07 \times 10^{-1}$	$1.25 \times 10^{+1}$	$1.15 \times 10^{+1}$
$2.83 \times 10^{-2}$	$1.28 \times 10^{+15}$	$1.02 \times 10^{-1}$	$2.38 \times 10^{+1}$	$1.89 \times 10^{+1}$
$4.21 \times 10^{-2}$	$2.20 \times 10^{+15}$	$6.89 \times 10^{-2}$	$2.82 \times 10^{+1}$	$2.14 \times 10^{+1}$
$5.00 \times 10^{-2}$	$2.76 \times 10^{+15}$	$5.81 \times 10^{-2}$	$3.13 \times 10^{+1}$	$2.29 \times 10^{+1}$
$7.10 \times 10^{-2}$	$4.71 \times 10^{+15}$	$4.08 \times 10^{-2}$	$3.54 \times 10^{+1}$	$2.49 \times 10^{+1}$
$7.47 \times 10^{-2}$	$5.05 \times 10^{+15}$	$3.88 \times 10^{-2}$	$3.60 \times 10^{+1}$	$2.53 \times 10^{+1}$
$1.15 \times 10^{-1}$	$1.04 \times 10^{+16}$	$2.53 \times 10^{-2}$	$3.93 \times 10^{+1}$	$2.71 \times 10^{+1}$
$1.52 \times 10^{-1}$	$1.68 \times 10^{+16}$	$1.91 \times 10^{-2}$	$4.18 \times 10^{+1}$	$2.79 \times 10^{+1}$
$1.71 \times 10^{-1}$	$2.12 \times 10^{+16}$	$1.69 \times 10^{-2}$	$4.29 \times 10^{+1}$	$2.80 \times 10^{+1}$
$1.77 \times 10^{-1}$	$2.27 \times 10^{+16}$	$1.64 \times 10^{-2}$	$4.35 \times 10^{+1}$	$2.80 \times 10^{+1}$
$1.78 \times 10^{-1}$	$2.37 \times 10^{+16}$	$1.63 \times 10^{-2}$	$4.39 \times 10^{+1}$	$2.89 \times 10^{+1}$
$1.78 \times 10^{-1}$	$3.02 \times 10^{+16}$	$1.63 \times 10^{-2}$	$4.44 \times 10^{+1}$	$2.93 \times 10^{+1}$
$4.44 \times 10^{-1}$	$1.19 \times 10^{+17}$	$6.53 \times 10^{-3}$	$4.96 \times 10^{+1}$	$3.45 \times 10^{+1}$
$5.52 \times 10^{-1}$	$1.77 \times 10^{+17}$	$5.26 \times 10^{-3}$	$5.26 \times 10^{+1}$	$3.58 \times 10^{+1}$
$7.53 \times 10^{-1}$	$3.13 \times 10^{+17}$	$3.85 \times 10^{-3}$	$5.72 \times 10^{+1}$	$3.77 \times 10^{+1}$

The detector is a home-built Bayert-Alpert-type ionization gauge, enclosed in an aluminium shell. The design of the ionization gauge is similar to that used by Buckman *et al* (1993). A dual-filament arrangement was used to provide a back-up filament in case one filament burned out. The filaments 0.005 inch in diameter and approximately 1 inch long were made of rhenium. The hole in the ionization gauge was initially 0.5 mm in diameter and later was increased to 0.8 mm in diameter when a replacement detector was made to substitute for the original one. The main reason was to observe the effect of the angular resolution of the detector on the profiles, but the change was also intended to increase

the ion signal and afford quicker pump down times in the experiment. The detector was rotated about the centre of the gas beam source, at a distance,  $r$ , of 30 mm from the centre of the tube exit. To compensate for the reduction in angular resolution with the replacement ionization gauge, it was moved further from the source exit (to  $r = 45$  mm) than it had been in the earlier one. However, to measure the intensity of weak sources at low pressure, the gauge was kept at  $r = 30$  mm or  $r$  was reduced to 25 mm. With these configurations, the resolution of the system was typically  $1^\circ$  to  $2^\circ$  FWHM. The ionization gauge could be adjusted in the plane of rotation to align it with the gas beam source.

**Table 5.** The same as table 4 but for molecular gases.

H <sub>2</sub>				
$P$ (Torr)	$dN/dt$ (s <sup>-1</sup> )	$\lambda$ (cm)	$\theta_{1/2}$ (deg)	$\theta_{1/2}^c$ (deg)
$1.00 \times 10^{-2}$	$2.59 \times 10^{+15}$	$9.28 \times 10^{-1}$	$1.04 \times 10^{+1}$	$1.00 \times 10^{+1}$
$1.29 \times 10^{-2}$	$3.67 \times 10^{+15}$	$7.22 \times 10^{-1}$	$1.05 \times 10^{+1}$	$1.04 \times 10^{+1}$
$1.71 \times 10^{-2}$	$5.49 \times 10^{+15}$	$5.43 \times 10^{-1}$	$1.10 \times 10^{+1}$	$1.08 \times 10^{+1}$
$2.21 \times 10^{-2}$	$8.06 \times 10^{+15}$	$4.22 \times 10^{-1}$	$1.25 \times 10^{+1}$	$1.16 \times 10^{+1}$
$2.60 \times 10^{-2}$	$9.96 \times 10^{+15}$	$3.58 \times 10^{-1}$	$1.36 \times 10^{+1}$	$1.23 \times 10^{+1}$
$2.86 \times 10^{-2}$	$1.16 \times 10^{+16}$	$3.26 \times 10^{-1}$	$1.39 \times 10^{+1}$	$1.35 \times 10^{+1}$
$3.32 \times 10^{-2}$	$1.38 \times 10^{+16}$	$2.81 \times 10^{-1}$	$1.56 \times 10^{+1}$	$1.37 \times 10^{+1}$
$5.06 \times 10^{-2}$	$2.52 \times 10^{+16}$	$1.84 \times 10^{-1}$	$1.86 \times 10^{+1}$	$1.57 \times 10^{+1}$
$7.97 \times 10^{-2}$	$4.74 \times 10^{+16}$	$1.17 \times 10^{-1}$	$2.20 \times 10^{+1}$	$1.79 \times 10^{+1}$
$9.57 \times 10^{-2}$	$5.95 \times 10^{+16}$	$9.73 \times 10^{-2}$	$2.54 \times 10^{+1}$	$1.93 \times 10^{+1}$
$1.07 \times 10^{-1}$	$7.16 \times 10^{+16}$	$8.67 \times 10^{-2}$	$2.64 \times 10^{+1}$	$1.99 \times 10^{+1}$
$1.32 \times 10^{-1}$	$9.67 \times 10^{+16}$	$7.06 \times 10^{-2}$	$3.00 \times 10^{+1}$	$2.21 \times 10^{+1}$
$1.50 \times 10^{-1}$	$1.25 \times 10^{+17}$	$6.19 \times 10^{-2}$	$2.97 \times 10^{+1}$	$2.22 \times 10^{+1}$
$1.75 \times 10^{-1}$	$1.51 \times 10^{+17}$	$5.33 \times 10^{-2}$	$3.22 \times 10^{+1}$	$2.29 \times 10^{+1}$
$2.83 \times 10^{-1}$	$3.42 \times 10^{+17}$	$3.29 \times 10^{-2}$	$3.74 \times 10^{+1}$	$2.57 \times 10^{+1}$
$3.29 \times 10^{-1}$	$4.51 \times 10^{+17}$	$2.83 \times 10^{-2}$	$3.80 \times 10^{+1}$	$2.59 \times 10^{+1}$
$4.07 \times 10^{-1}$	$6.25 \times 10^{+17}$	$2.29 \times 10^{-2}$	$3.98 \times 10^{+1}$	$2.72 \times 10^{+1}$
N <sub>2</sub>				
$P$ (Torr)	$dN/dt$ (s <sup>-1</sup> )	$\lambda$ (cm)	$\theta_{1/2}$ (deg)	$\theta_{1/2}^c$ (deg)
$1.52 \times 10^{-3}$	$1.05 \times 10^{+14}$	$3.26 \times 10^0$	$7.75 \times 10^0$	$7.50 \times 10^0$
$5.17 \times 10^{-3}$	$3.50 \times 10^{+14}$	$9.62 \times 10^{-1}$	$1.02 \times 10^{+1}$	$9.60 \times 10^0$
$8.52 \times 10^{-3}$	$4.67 \times 10^{+14}$	$5.84 \times 10^{-1}$	$1.12 \times 10^{+1}$	$1.05 \times 10^{+1}$
$9.74 \times 10^{-3}$	$6.74 \times 10^{+14}$	$5.11 \times 10^{-1}$	$1.22 \times 10^{+1}$	$1.13 \times 10^{+1}$
$1.17 \times 10^{-2}$	$8.58 \times 10^{+14}$	$4.25 \times 10^{-1}$	$1.32 \times 10^{+1}$	$1.22 \times 10^{+1}$
$1.47 \times 10^{-2}$	$9.04 \times 10^{+14}$	$3.38 \times 10^{-1}$	$1.42 \times 10^{+1}$	$1.27 \times 10^{+1}$
$1.83 \times 10^{-2}$	$1.30 \times 10^{+15}$	$2.72 \times 10^{-1}$	$1.61 \times 10^{+1}$	$1.42 \times 10^{+1}$
$2.20 \times 10^{-2}$	$1.44 \times 10^{+15}$	$2.26 \times 10^{-1}$	$1.70 \times 10^{+1}$	$1.49 \times 10^{+1}$
$3.06 \times 10^{-2}$	$2.41 \times 10^{+15}$	$1.63 \times 10^{-1}$	$2.01 \times 10^{+1}$	$1.68 \times 10^{+1}$
$4.16 \times 10^{-2}$	$3.70 \times 10^{+15}$	$1.19 \times 10^{-1}$	$2.32 \times 10^{+1}$	$1.85 \times 10^{+1}$
$5.28 \times 10^{-2}$	$5.36 \times 10^{+15}$	$9.42 \times 10^{-2}$	$2.67 \times 10^{+1}$	$2.04 \times 10^{+1}$
$7.46 \times 10^{-2}$	$8.27 \times 10^{+15}$	$6.66 \times 10^{-2}$	$3.05 \times 10^{+1}$	$2.25 \times 10^{+1}$
$8.31 \times 10^{-2}$	$1.03 \times 10^{+16}$	$5.98 \times 10^{-2}$	$3.23 \times 10^{+1}$	$2.33 \times 10^{+1}$
$1.03 \times 10^{-1}$	$1.37 \times 10^{+16}$	$4.82 \times 10^{-2}$	$3.47 \times 10^{+1}$	$2.46 \times 10^{+1}$
$1.13 \times 10^{-1}$	$1.65 \times 10^{+16}$	$4.39 \times 10^{-2}$	$3.62 \times 10^{+1}$	$2.51 \times 10^{+1}$
$1.39 \times 10^{-1}$	$2.33 \times 10^{+16}$	$3.57 \times 10^{-2}$	$3.85 \times 10^{+1}$	$2.63 \times 10^{+1}$
$1.89 \times 10^{-1}$	$3.82 \times 10^{+16}$	$2.64 \times 10^{-2}$	$4.01 \times 10^{+1}$	$2.83 \times 10^{+1}$
$2.49 \times 10^{-1}$	$6.35 \times 10^{+16}$	$2.00 \times 10^{-2}$	$4.25 \times 10^{+1}$	$3.16 \times 10^{+1}$
$2.71 \times 10^{-1}$	$7.15 \times 10^{+16}$	$1.84 \times 10^{-2}$	$4.48 \times 10^{+1}$	$3.16 \times 10^{+1}$
$3.21 \times 10^{-1}$	$9.51 \times 10^{+16}$	$1.55 \times 10^{-2}$	$4.63 \times 10^{+1}$	$3.40 \times 10^{+1}$

The back plate of the gauge contained the relevant electrical feedthroughs (insulated with steatite) for the gauge as well as a central tapped hole for alignment of the ionization gauge detector with the gas tube source. This was closed during operation, using a screw. By running the experiment with the gauge alignment hole closed, the sensitivity of the gauge is improved (Adamson and McGilp 1986, Buckman *et al* 1993). The filament was operated at the ground potential of the vacuum tank, with the grid at 100 V positive and the collector at 20 V negative relative to the filament ground. Typical signal-to-background current ratios ranged from 1:3 to 1:1.

The computer data acquisition system used interrogated a digital voltmeter via an IEEE bus to read various voltages associated with the experiment via a home-built multiplexer. The computer also controlled the angular displacement of the ionization gauge gas detector via a stepper motor which turned a rigid-shaft rotary feedthrough. The angle of the

detector was determined from the voltage across a standard one-turn Allen-Bradley 10 k $\Omega$  potentiometer attached to the rotary feedthrough and powered by a 5 V regulated power supply. This system was calibrated *in situ* using a protractor and the potentiometer voltage reading as a function of angular displacement was fitted to a third-order polynomial to allow for a small non-linearity in the angular behaviour of the potentiometer. This set-up allowed the computer to accurately locate angles to better than  $\pm 0.5^\circ$  using a computer controlled voltmeter. The performance and method of alignment of our system were checked by using an aperture ( $\cos \theta$  distribution) source in place of the effusive tubes. The agreement was found to be excellent (see figure 2). From this calibration, we estimate the detection accuracy of our profiles (the vertical axis in figure 2) to be within around 2.0%.

Two gas-collimating structures were used. The first was a single-capillary source of internal diameter  $d = 0.08$  cm

**Table 5.** (Continued)

$C_2H_2$				
$P$ (Torr)	$dN/dt$ ( $s^{-1}$ )	$\lambda$ (cm)	$\theta_{1/2}$ (deg)	$\theta_{1/2}^c$ (deg)
$2.19 \times 10^{-3}$	$1.26 \times 10^{14}$	$1.27 \times 10^0$	$1.00 \times 10^{+1}$	$1.15 \times 10^{+1}$
$3.76 \times 10^{-3}$	$3.35 \times 10^{14}$	$7.44 \times 10^{-1}$	$1.10 \times 10^{+1}$	$1.15 \times 10^{+1}$
$4.09 \times 10^{-3}$	$3.18 \times 10^{14}$	$6.84 \times 10^{-1}$	$1.22 \times 10^{+1}$	$1.18 \times 10^{+1}$
$6.55 \times 10^{-3}$	$5.14 \times 10^{14}$	$4.27 \times 10^{-1}$	$1.30 \times 10^{+1}$	$1.19 \times 10^{+1}$
$8.64 \times 10^{-3}$	$5.45 \times 10^{14}$	$3.24 \times 10^{-1}$	$1.50 \times 10^{+1}$	$1.45 \times 10^{+1}$
$1.10 \times 10^{-2}$	$8.50 \times 10^{14}$	$2.54 \times 10^{-1}$	$1.66 \times 10^{+1}$	$1.48 \times 10^{+1}$
$2.54 \times 10^{-2}$	$2.19 \times 10^{15}$	$1.10 \times 10^{-1}$	$2.47 \times 10^{+1}$	$1.95 \times 10^{+1}$
$3.05 \times 10^{-2}$	$2.56 \times 10^{15}$	$9.17 \times 10^{-2}$	$2.65 \times 10^{+1}$	$2.05 \times 10^{+1}$
$4.02 \times 10^{-2}$	$3.86 \times 10^{15}$	$6.95 \times 10^{-2}$	$3.05 \times 10^{+1}$	$2.21 \times 10^{+1}$
$7.46 \times 10^{-2}$	$1.02 \times 10^{16}$	$3.75 \times 10^{-2}$	$3.49 \times 10^{+1}$	$2.65 \times 10^{+1}$
$8.58 \times 10^{-2}$	$1.22 \times 10^{16}$	$3.26 \times 10^{-2}$	$3.79 \times 10^{+1}$	$2.62 \times 10^{+1}$
$9.14 \times 10^{-2}$	$1.38 \times 10^{16}$	$3.06 \times 10^{-2}$	$3.91 \times 10^{+1}$	$2.63 \times 10^{+1}$
$1.14 \times 10^{-1}$	$1.96 \times 10^{16}$	$2.45 \times 10^{-2}$	$4.09 \times 10^{+1}$	$2.73 \times 10^{+1}$
$1.71 \times 10^{-1}$	$3.89 \times 10^{16}$	$1.63 \times 10^{-2}$	$4.48 \times 10^{+1}$	$2.88 \times 10^{+1}$
$CO_2$				
$P$ (Torr)	$dN/dt$ ( $s^{-1}$ )	$\lambda$ (cm)	$\theta_{1/2}$ (deg)	$\theta_{1/2}^c$ (deg)
$2.10 \times 10^{-3}$	$1.06 \times 10^{14}$	$1.54 \times 10^0$	$1.00 \times 10^{+1}$	$9.80 \times 10^0$
$4.05 \times 10^{-3}$	$2.74 \times 10^{14}$	$7.98 \times 10^{-1}$	$1.10 \times 10^{+1}$	$1.12 \times 10^{+1}$
$8.76 \times 10^{-3}$	$5.57 \times 10^{14}$	$3.69 \times 10^{-1}$	$1.20 \times 10^{+1}$	$1.31 \times 10^{+1}$
$1.20 \times 10^{-2}$	$8.51 \times 10^{14}$	$2.70 \times 10^{-1}$	$1.35 \times 10^{+1}$	$1.43 \times 10^{+1}$
$1.91 \times 10^{-2}$	$1.49 \times 10^{15}$	$1.69 \times 10^{-1}$	$2.02 \times 10^{+1}$	$1.71 \times 10^{+1}$
$3.45 \times 10^{-2}$	$2.89 \times 10^{15}$	$9.38 \times 10^{-2}$	$2.54 \times 10^{+1}$	$2.03 \times 10^{+1}$
$3.78 \times 10^{-2}$	$3.15 \times 10^{15}$	$8.57 \times 10^{-2}$	$2.71 \times 10^{+1}$	$2.06 \times 10^{+1}$
$4.20 \times 10^{-2}$	$3.73 \times 10^{15}$	$7.70 \times 10^{-2}$	$2.78 \times 10^{+1}$	$2.13 \times 10^{+1}$
$5.26 \times 10^{-2}$	$5.33 \times 10^{15}$	$6.15 \times 10^{-2}$	$3.11 \times 10^{+1}$	$2.32 \times 10^{+1}$
$5.56 \times 10^{-2}$	$5.53 \times 10^{15}$	$5.82 \times 10^{-2}$	$3.06 \times 10^{+1}$	$2.27 \times 10^{+1}$
$6.16 \times 10^{-2}$	$6.75 \times 10^{15}$	$5.25 \times 10^{-2}$	$3.28 \times 10^{+1}$	$2.38 \times 10^{+1}$
$7.49 \times 10^{-2}$	$8.67 \times 10^{15}$	$4.32 \times 10^{-2}$	$3.33 \times 10^{+1}$	$2.47 \times 10^{+1}$
$7.68 \times 10^{-2}$	$9.39 \times 10^{15}$	$4.21 \times 10^{-2}$	$3.38 \times 10^{+1}$	$2.50 \times 10^{+1}$
$1.14 \times 10^{-1}$	$1.70 \times 10^{16}$	$2.84 \times 10^{-2}$	$3.89 \times 10^{+1}$	$2.69 \times 10^{+1}$
$1.67 \times 10^{-1}$	$3.27 \times 10^{16}$	$1.94 \times 10^{-2}$	$4.24 \times 10^{+1}$	$2.84 \times 10^{+1}$
$2.13 \times 10^{-1}$	$5.13 \times 10^{16}$	$1.52 \times 10^{-2}$	$4.41 \times 10^{+1}$	$3.09 \times 10^{+1}$
$2.51 \times 10^{-1}$	$6.89 \times 10^{16}$	$1.29 \times 10^{-2}$	$4.58 \times 10^{+1}$	$3.33 \times 10^{+1}$

**Table 6.** The same as table 3, but for the multi-capillary tube source.

Gas	$M$	$\delta$	$a$	$\Delta a$	$\varepsilon$	$\Delta \varepsilon$	$\delta_R$	$\Delta \delta_R$
H <sub>2</sub>	2	2.74	8875	428	0.33	0.06	2.74	0.77
He	4	2.18	6075	491	0.21	0.05		
Ne	20.2	2.60	2623	167	0.29	0.06	2.74	0.79
C <sub>2</sub> H <sub>2</sub>	26	5.00	2225	187	1.14	0.14	4.66	1.25
N <sub>2</sub>	28	3.75	2266	176	0.61	0.08	3.46	0.93
Ar	39.9	3.64	1940	182	0.57	0.10	3.59	1.01
Xe	131	4.91	1021	150	1.05	0.19	4.40	1.38

and length  $L = 2$  cm, i.e. an aspect ratio  $\gamma (= D/L)$  of 0.04, and the second was a multi-capillary source made up of 91 tubes in a circular matrix of 0.9 mm diameter. Each tube was nominally 0.00508 cm in diameter and of length 0.508 cm ( $\gamma = 0.01$ ). The multi-capillary source was mounted at the end of a stainless steel hypodermic needle. A schematic diagram of the gas handling system is shown in figure 3. All-metal tubing, metal regulator diaphragms and metal bellows valves were used. This allowed the gas system, in the region after the fine-metering leak valve LV (see figure 3), to be evacuated to  $<10^{-5}$  Torr. The pressure,

$P$ , in the source feed line was monitored using an absolute capacitance manometer, a baratron, B (figure 3).

The procedure by which data was acquired was as follows.

- (i) Firstly, with valves SV and BV opened (valves VV and RV shut), the leak valve LV was opened by a required amount and the system allowed to equilibrate. The equilibrium vacuum tank pressure was recorded by a commercial ionization gauge. Valves SV and BV were closed simultaneously and the computer was made to read the capacitance manometer at uniform time

**Table 7.** A summary of measurements for atomic gases using the multi-capillary source, with  $D = 0.00508$  cm and  $L = 0.508$  cm. See the text for descriptions of parameters.

He				
$P$ (Torr)	$dN/dt$ ( $s^{-1}$ )	$\lambda$ (cm)	$\theta_{1/2}$ (deg)	$\theta_{1/2}^c$ (deg)
$8.42 \times 10^{-3}$	$4.65 \times 10^{14}$	$1.75 \times 10^0$	$4.30 \times 10^0$	$3.70 \times 10^0$
$1.17 \times 10^{-2}$	$4.61 \times 10^{14}$	$1.26 \times 10^0$	$4.60 \times 10^0$	$3.70 \times 10^0$
$3.97 \times 10^{-2}$	$2.35 \times 10^{15}$	$3.71 \times 10^{-1}$	$4.70 \times 10^0$	$4.37 \times 10^0$
$7.02 \times 10^{-2}$	$4.29 \times 10^{15}$	$2.10 \times 10^{-1}$	$5.15 \times 10^0$	$4.74 \times 10^0$
$8.69 \times 10^{-2}$	$4.79 \times 10^{15}$	$1.69 \times 10^{-1}$	$5.35 \times 10^0$	$4.89 \times 10^0$
$9.26 \times 10^{-2}$	$5.66 \times 10^{15}$	$1.59 \times 10^{-1}$	$5.75 \times 10^0$	$4.69 \times 10^0$
$1.21 \times 10^{-1}$	$7.69 \times 10^{15}$	$1.22 \times 10^{-1}$	$6.15 \times 10^0$	$5.07 \times 10^0$
$1.30 \times 10^{-1}$	$8.62 \times 10^{15}$	$1.13 \times 10^{-1}$	$5.70 \times 10^0$	$5.56 \times 10^0$
$1.54 \times 10^{-1}$	$9.81 \times 10^{15}$	$9.54 \times 10^{-2}$	$5.80 \times 10^0$	$5.70 \times 10^0$
$2.03 \times 10^{-1}$	$1.34 \times 10^{16}$	$7.24 \times 10^{-2}$	$6.50 \times 10^0$	$6.49 \times 10^0$
$4.06 \times 10^{-1}$	$2.82 \times 10^{16}$	$3.62 \times 10^{-2}$	$9.70 \times 10^0$	$9.16 \times 10^0$
$4.34 \times 10^{-1}$	$3.02 \times 10^{16}$	$3.39 \times 10^{-2}$	$9.60 \times 10^0$	$9.06 \times 10^0$
$6.88 \times 10^{-1}$	$5.03 \times 10^{16}$	$2.14 \times 10^{-2}$	$1.38 \times 10^1$	$1.19 \times 10^1$
$7.99 \times 10^{-1}$	$5.91 \times 10^{16}$	$1.84 \times 10^{-2}$	$1.59 \times 10^1$	$1.28 \times 10^1$
$1.10 \times 10^0$	$8.34 \times 10^{16}$	$1.34 \times 10^{-2}$	$1.89 \times 10^1$	$1.45 \times 10^1$
$1.33 \times 10^0$	$1.04 \times 10^{17}$	$1.11 \times 10^{-2}$	$2.22 \times 10^1$	$1.62 \times 10^1$
$1.95 \times 10^0$	$1.55 \times 10^{17}$	$7.55 \times 10^{-3}$	$2.87 \times 10^1$	$1.99 \times 10^1$
$2.29 \times 10^0$	$1.97 \times 10^{17}$	$6.42 \times 10^{-3}$	$2.93 \times 10^1$	$2.07 \times 10^1$
Ne				
$P$ (Torr)	$dN/dt$ ( $s^{-1}$ )	$\lambda$ (cm)	$\theta_{1/2}$ (deg)	$\theta_{1/2}^c$ (deg)
$6.99 \times 10^{-3}$	$2.00 \times 10^{14}$	$1.48 \times 10^0$	$4.45 \times 10^0$	$4.40 \times 10^0$
$1.11 \times 10^{-2}$	$3.22 \times 10^{14}$	$9.36 \times 10^{-1}$	$4.35 \times 10^0$	$4.28 \times 10^0$
$1.41 \times 10^{-2}$	$3.84 \times 10^{14}$	$7.32 \times 10^{-1}$	$4.40 \times 10^0$	$4.41 \times 10^0$
$2.09 \times 10^{-2}$	$6.96 \times 10^{14}$	$4.96 \times 10^{-1}$	$5.25 \times 10^0$	$5.01 \times 10^0$
$3.40 \times 10^{-2}$	$9.77 \times 10^{14}$	$3.04 \times 10^{-1}$	$5.10 \times 10^0$	$4.70 \times 10^0$
$3.46 \times 10^{-2}$	$1.01 \times 10^{15}$	$2.99 \times 10^{-1}$	$5.55 \times 10^0$	$5.13 \times 10^0$
$6.09 \times 10^{-2}$	$1.83 \times 10^{15}$	$1.70 \times 10^{-1}$	$5.70 \times 10^0$	$5.40 \times 10^0$
$6.50 \times 10^{-2}$	$1.71 \times 10^{15}$	$1.59 \times 10^{-1}$	$5.70 \times 10^0$	$5.43 \times 10^0$
$7.18 \times 10^{-2}$	$2.12 \times 10^{15}$	$1.44 \times 10^{-1}$	$6.10 \times 10^0$	$5.28 \times 10^0$
$8.27 \times 10^{-2}$	$2.68 \times 10^{15}$	$1.25 \times 10^{-1}$	$6.90 \times 10^0$	$5.66 \times 10^0$
$8.88 \times 10^{-2}$	$2.46 \times 10^{15}$	$1.17 \times 10^{-1}$	$5.95 \times 10^0$	$5.55 \times 10^0$
$1.02 \times 10^{-1}$	$3.30 \times 10^{15}$	$1.02 \times 10^{-1}$	$7.30 \times 10^0$	$6.30 \times 10^0$
$1.22 \times 10^{-1}$	$3.34 \times 10^{15}$	$8.51 \times 10^{-2}$	$7.60 \times 10^0$	$6.54 \times 10^0$
$1.28 \times 10^{-1}$	$3.81 \times 10^{15}$	$8.09 \times 10^{-2}$	$7.50 \times 10^0$	$7.00 \times 10^0$
$1.54 \times 10^{-1}$	$4.73 \times 10^{15}$	$6.71 \times 10^{-2}$	$8.10 \times 10^0$	$7.30 \times 10^0$
$1.97 \times 10^{-1}$	$5.56 \times 10^{15}$	$5.25 \times 10^{-2}$	$9.40 \times 10^0$	$8.54 \times 10^0$
$2.47 \times 10^{-1}$	$6.96 \times 10^{15}$	$4.20 \times 10^{-2}$	$1.07 \times 10^1$	$9.26 \times 10^0$
$2.76 \times 10^{-1}$	$7.82 \times 10^{15}$	$3.75 \times 10^{-2}$	$1.13 \times 10^1$	$1.01 \times 10^1$
$3.50 \times 10^{-1}$	$1.01 \times 10^{16}$	$2.96 \times 10^{-2}$	$1.33 \times 10^1$	$1.06 \times 10^1$
$4.34 \times 10^{-1}$	$1.29 \times 10^{16}$	$2.39 \times 10^{-2}$	$1.57 \times 10^1$	$1.26 \times 10^1$
$6.57 \times 10^{-1}$	$2.09 \times 10^{16}$	$1.58 \times 10^{-2}$	$1.92 \times 10^1$	$1.49 \times 10^1$
$6.82 \times 10^{-1}$	$2.17 \times 10^{16}$	$1.52 \times 10^{-2}$	$2.05 \times 10^1$	$1.55 \times 10^1$
$8.46 \times 10^{-1}$	$2.79 \times 10^{16}$	$1.22 \times 10^{-2}$	$2.22 \times 10^1$	$1.74 \times 10^1$
$1.15 \times 10^0$	$4.87 \times 10^{16}$	$8.98 \times 10^{-3}$	$2.68 \times 10^1$	$1.97 \times 10^1$
$1.25 \times 10^0$	$5.40 \times 10^{16}$	$8.29 \times 10^{-3}$	$2.84 \times 10^1$	$2.13 \times 10^1$
$1.79 \times 10^0$	$7.95 \times 10^{16}$	$5.77 \times 10^{-3}$	$3.13 \times 10^1$	$2.39 \times 10^1$
$2.77 \times 10^0$	$1.29 \times 10^{17}$	$3.73 \times 10^{-3}$	$3.44 \times 10^1$	$2.89 \times 10^1$
$2.80 \times 10^0$	$1.33 \times 10^{17}$	$3.70 \times 10^{-3}$	$3.51 \times 10^1$	$2.95 \times 10^1$
$3.10 \times 10^0$	$1.52 \times 10^{17}$	$3.33 \times 10^{-3}$	$3.62 \times 10^1$	$3.07 \times 10^1$
$4.19 \times 10^0$	$2.26 \times 10^{17}$	$2.47 \times 10^{-3}$	$3.78 \times 10^1$	$3.23 \times 10^1$
$4.98 \times 10^0$	$2.95 \times 10^{17}$	$2.08 \times 10^{-3}$	$3.93 \times 10^1$	$3.41 \times 10^1$

intervals (1 s or less) to observe the linear rise in pressure  $P$  versus time. From the linear slope of  $P$  versus  $t$ ,  $dP/dt$ , we could derive the flow rate of gas as

$$\frac{dN}{dt} = \dot{N} = \frac{V}{kT} \frac{dP}{dt} \quad (4)$$

where  $V$  is the volume of space enclosed by the valves BV, LV, RV and SV.  $V$  was determined by comparing it against a standard volume ( $V_0$ ) (filling gas either in  $V$  or  $V_0$  and opening VV while observing the reading of B). This procedure allowed us to determine  $\dot{N}$  using a laboratory temperature,  $T$ , of 300 K.

Table 7. (Continued)

Ar				
$P$ (Torr)	$dN/dt$ ( $s^{-1}$ )	$\lambda$ (cm)	$\theta_{1/2}$ (deg)	$\theta_{1/2}^c$ (deg)
$4.09 \times 10^{-3}$	$6.24 \times 10^{+13}$	$1.29 \times 10^0$	$4.15 \times 10^0$	$4.00 \times 10^0$
$8.32 \times 10^{-3}$	$1.27 \times 10^{+14}$	$6.34 \times 10^{-1}$	$4.62 \times 10^0$	$4.13 \times 10^0$
$8.49 \times 10^{-3}$	$1.35 \times 10^{+14}$	$6.22 \times 10^{-1}$	$4.60 \times 10^0$	$4.20 \times 10^0$
$1.86 \times 10^{-2}$	$3.91 \times 10^{+14}$	$2.85 \times 10^{-1}$	$5.50 \times 10^0$	$4.80 \times 10^0$
$2.73 \times 10^{-2}$	$5.15 \times 10^{+14}$	$1.94 \times 10^{-1}$	$6.25 \times 10^0$	$5.85 \times 10^0$
$6.03 \times 10^{-2}$	$1.15 \times 10^{+15}$	$8.75 \times 10^{-2}$	$7.70 \times 10^0$	$6.50 \times 10^0$
$9.21 \times 10^{-2}$	$1.75 \times 10^{+15}$	$5.73 \times 10^{-2}$	$8.70 \times 10^0$	$7.40 \times 10^0$
$1.37 \times 10^{-1}$	$2.74 \times 10^{+15}$	$3.86 \times 10^{-2}$	$1.01 \times 10^{+1}$	$8.70 \times 10^0$
$1.70 \times 10^{-1}$	$3.56 \times 10^{+15}$	$3.11 \times 10^{-2}$	$1.27 \times 10^{+1}$	$9.45 \times 10^0$
$1.70 \times 10^{-1}$	$3.34 \times 10^{+15}$	$3.11 \times 10^{-2}$	$1.34 \times 10^{+1}$	$1.18 \times 10^{+1}$
$2.43 \times 10^{-1}$	$5.60 \times 10^{+15}$	$2.18 \times 10^{-2}$	$1.64 \times 10^{+1}$	$1.23 \times 10^{+1}$
$4.00 \times 10^{-1}$	$9.10 \times 10^{+15}$	$1.32 \times 10^{-2}$	$2.05 \times 10^{+1}$	$1.43 \times 10^{+1}$
$4.16 \times 10^{-1}$	$9.64 \times 10^{+15}$	$1.27 \times 10^{-2}$	$2.29 \times 10^{+1}$	$1.59 \times 10^{+1}$
$5.79 \times 10^{-1}$	$1.51 \times 10^{+16}$	$9.12 \times 10^{-3}$	$2.74 \times 10^{+1}$	$1.82 \times 10^{+1}$
$6.74 \times 10^{-1}$	$1.80 \times 10^{+16}$	$7.84 \times 10^{-3}$	$2.91 \times 10^{+1}$	$1.98 \times 10^{+1}$
$7.87 \times 10^{-1}$	$2.22 \times 10^{+16}$	$6.71 \times 10^{-3}$	$3.06 \times 10^{+1}$	$2.27 \times 10^{+1}$
$1.73 \times 10^0$	$4.99 \times 10^{+16}$	$3.05 \times 10^{-3}$	$3.85 \times 10^{+1}$	$3.12 \times 10^{+1}$
$4.95 \times 10^0$	$2.01 \times 10^{+17}$	$1.07 \times 10^{-3}$	$5.13 \times 10^{+1}$	$4.16 \times 10^{+1}$
Xe				
$P$ (Torr)	$dN/dt$ ( $s^{-1}$ )	$\lambda$ (cm)	$\theta_{1/2}$ (deg)	$\theta_{1/2}^c$ (deg)
$2.14 \times 10^{-3}$	$2.36 \times 10^{+13}$	$1.35 \times 10^0$	$4.40 \times 10^0$	$3.75 \times 10^0$
$6.99 \times 10^{-3}$	$7.81 \times 10^{+13}$	$4.15 \times 10^{-1}$	$4.35 \times 10^0$	$4.35 \times 10^0$
$7.14 \times 10^{-3}$	$7.08 \times 10^{+13}$	$4.06 \times 10^{-1}$	$4.25 \times 10^0$	$4.20 \times 10^0$
$1.48 \times 10^{-2}$	$1.73 \times 10^{+14}$	$1.96 \times 10^{-1}$	$5.45 \times 10^0$	$5.30 \times 10^0$
$3.88 \times 10^{-2}$	$3.87 \times 10^{+14}$	$7.48 \times 10^{-2}$	$7.85 \times 10^0$	$7.55 \times 10^0$
$4.83 \times 10^{-2}$	$5.02 \times 10^{+14}$	$6.00 \times 10^{-2}$	$8.60 \times 10^0$	$8.25 \times 10^0$
$5.66 \times 10^{-2}$	$6.05 \times 10^{+14}$	$5.13 \times 10^{-2}$	$9.25 \times 10^0$	$8.85 \times 10^0$
$9.41 \times 10^{-2}$	$1.02 \times 10^{+15}$	$3.08 \times 10^{-2}$	$1.18 \times 10^{+1}$	$1.07 \times 10^{+1}$
$1.37 \times 10^{-1}$	$1.52 \times 10^{+15}$	$2.12 \times 10^{-2}$	$1.51 \times 10^{+1}$	$1.27 \times 10^{+1}$
$1.54 \times 10^{-1}$	$1.71 \times 10^{+15}$	$1.89 \times 10^{-2}$	$1.62 \times 10^{+1}$	$1.36 \times 10^{+1}$
$1.72 \times 10^{-1}$	$1.93 \times 10^{+15}$	$1.68 \times 10^{-2}$	$1.81 \times 10^{+1}$	$1.40 \times 10^{+1}$
$2.04 \times 10^{-1}$	$2.47 \times 10^{+15}$	$1.42 \times 10^{-2}$	$1.95 \times 10^{+1}$	$1.50 \times 10^{+1}$
$3.09 \times 10^{-1}$	$3.91 \times 10^{+15}$	$9.39 \times 10^{-3}$	$2.50 \times 10^{+1}$	$1.78 \times 10^{+1}$
$5.44 \times 10^{-1}$	$7.10 \times 10^{+15}$	$5.33 \times 10^{-3}$	$3.32 \times 10^{+1}$	$2.66 \times 10^{+1}$
$9.15 \times 10^{-1}$	$1.41 \times 10^{+16}$	$3.17 \times 10^{-3}$	$3.68 \times 10^{+1}$	$3.17 \times 10^{+1}$

(ii) SV and BV were opened and, after the pressure had dropped sufficiently, BV was closed and again, with the assistance of a computer, a  $P$  versus  $t$  graph was acquired and fitted to the equation (Khakoo *et al* 1993)

$$P(t) = P(\infty) + [P(0) - P(\infty)]e^{-\beta t} \quad (5)$$

where  $\beta$  is related to the pumping speed of the system (this is accurate to within  $\pm 1\%$  to first-order<sup>†</sup>).  $P(\infty)$  is the pressure at the capacitance manometer under equilibrium flow conditions. In general, the conductance of piping between the manometer and the gas capillary cannot be neglected and  $P$  is not the pressure immediately behind the capillary,  $P_s$ , but is linearly related to it. In the present case consideration of our tube conductances (Dushman 1949) (effectively a 55 cm length of 0.476 cm diameter tubing followed by the source needle) shows that  $P_s/P$  was approximately 0.85

<sup>†</sup> Sagara and Boesten (1998) recently performed an extensive study of the dependence of  $dN/dt$  on  $P$  (measured upstream from the gas source) and obtained a second-order correction to equation (5).

for the single-tube source, but 0.98 for the multi-channel capillary source (in the free-molecular flow regime). A typical measurement of  $P$  versus  $t$  carried out to determine  $dP/dt$  and  $P(\infty)$  from procedures (i) and (ii) is shown in figure 4.

(iii) The flow set in (ii) was allowed to equilibrate ( $P = P(\infty)$ ) and the gas beam detector (ionization gauge) was rotated about the source from  $\theta = -100^\circ$  to  $\theta = 100^\circ$ , stepping at  $5^\circ$  intervals for  $|\theta| > 20^\circ$  and at  $1^\circ$  intervals for  $|\theta| < 20^\circ$ . The gas beam intensity could usually be obtained in a single scan, but, at low pressures, several scans were necessary in order to reduce the uncertainty to within 2%.

Using this experimental set-up, we measured profiles for several pure gases as a function of the source pressure measured at the manometer and the flow rate. Illustrations of data taken with the tube source and the multi-capillary array, using argon gas, are shown in figures 5(a) and (b). Characteristic gas constants available for these gases are summarized in table 2.

**Table 8.** The same as table 7 but for molecular gases.

H <sub>2</sub>				
$P$ (Torr)	$dN/dt$ (s <sup>-1</sup> )	$\lambda$ (cm)	$\theta_{1/2}$ (deg)	$\theta_{1/2}^c$ (deg)
$5.60 \times 10^{-3}$	$4.54 \times 10^{14}$	$1.66 \times 10^0$	$4.90 \times 10^0$	$3.80 \times 10^0$
$1.10 \times 10^{-2}$	$7.42 \times 10^{14}$	$8.46 \times 10^{-1}$	$5.00 \times 10^0$	$4.10 \times 10^0$
$1.58 \times 10^{-2}$	$8.09 \times 10^{14}$	$5.88 \times 10^{-1}$	$5.00 \times 10^0$	$4.45 \times 10^0$
$1.37 \times 10^{-2}$	$8.52 \times 10^{14}$	$6.82 \times 10^{-1}$	$5.05 \times 10^0$	$4.34 \times 10^0$
$2.10 \times 10^{-2}$	$1.73 \times 10^{15}$	$4.43 \times 10^{-1}$	$4.85 \times 10^0$	$4.77 \times 10^0$
$5.18 \times 10^{-2}$	$4.25 \times 10^{15}$	$1.80 \times 10^{-1}$	$5.65 \times 10^0$	$5.53 \times 10^0$
$6.73 \times 10^{-2}$	$5.65 \times 10^{15}$	$1.38 \times 10^{-1}$	$5.85 \times 10^0$	$5.62 \times 10^0$
$6.74 \times 10^{-2}$	$5.02 \times 10^{15}$	$1.38 \times 10^{-1}$	$5.95 \times 10^0$	$5.78 \times 10^0$
$1.87 \times 10^{-1}$	$1.70 \times 10^{16}$	$4.99 \times 10^{-2}$	$8.00 \times 10^0$	$8.61 \times 10^0$
$2.70 \times 10^{-1}$	$2.58 \times 10^{16}$	$3.45 \times 10^{-2}$	$1.11 \times 10^{+1}$	$1.00 \times 10^{+1}$
$3.94 \times 10^{-1}$	$3.83 \times 10^{16}$	$2.36 \times 10^{-2}$	$1.45 \times 10^{+1}$	$1.17 \times 10^{+1}$
$4.99 \times 10^{-1}$	$5.15 \times 10^{16}$	$1.87 \times 10^{-2}$	$1.56 \times 10^{+1}$	$1.34 \times 10^{+1}$
$6.52 \times 10^{-1}$	$6.84 \times 10^{16}$	$1.43 \times 10^{-2}$	$2.01 \times 10^{+1}$	$1.42 \times 10^{+1}$
$7.25 \times 10^{-1}$	$7.67 \times 10^{16}$	$1.28 \times 10^{-2}$	$2.16 \times 10^{+1}$	$1.60 \times 10^{+1}$
$9.79 \times 10^{-1}$	$1.08 \times 10^{17}$	$9.52 \times 10^{-3}$	$2.58 \times 10^{+1}$	$1.83 \times 10^{+1}$
$1.23 \times 10^0$	$1.39 \times 10^{17}$	$7.58 \times 10^{-3}$	$2.88 \times 10^{+1}$	$2.04 \times 10^{+1}$
$1.69 \times 10^0$	$2.09 \times 10^{17}$	$5.50 \times 10^{-3}$	$3.21 \times 10^{+1}$	$2.31 \times 10^{+1}$
$1.99 \times 10^0$	$2.52 \times 10^{17}$	$4.68 \times 10^{-3}$	$3.22 \times 10^{+1}$	$2.48 \times 10^{+1}$
$2.33 \times 10^0$	$3.44 \times 10^{17}$	$4.00 \times 10^{-3}$	$3.50 \times 10^{+1}$	$2.72 \times 10^{+1}$
N <sub>2</sub>				
$P$ (Torr)	$dN/dt$ (s <sup>-1</sup> )	$\lambda$ (cm)	$\theta_{1/2}$ (deg)	$\theta_{1/2}^c$ (deg)
$4.40 \times 10^{-3}$	$4.94 \times 10^{13}$	$1.13 \times 10^0$	$4.40 \times 10^0$	$3.57 \times 10^0$
$6.10 \times 10^{-3}$	$6.64 \times 10^{13}$	$8.15 \times 10^{-1}$	$4.40 \times 10^0$	$3.50 \times 10^0$
$7.20 \times 10^{-3}$	$8.13 \times 10^{13}$	$6.91 \times 10^{-1}$	$5.00 \times 10^0$	$4.60 \times 10^0$
$1.58 \times 10^{-2}$	$2.98 \times 10^{14}$	$3.15 \times 10^{-1}$	$5.60 \times 10^0$	$5.20 \times 10^0$
$1.86 \times 10^{-2}$	$3.07 \times 10^{14}$	$2.67 \times 10^{-1}$	$5.70 \times 10^0$	$5.30 \times 10^0$
$2.57 \times 10^{-2}$	$4.72 \times 10^{14}$	$1.93 \times 10^{-1}$	$6.00 \times 10^0$	$5.74 \times 10^0$
$4.38 \times 10^{-2}$	$9.09 \times 10^{14}$	$1.14 \times 10^{-1}$	$6.35 \times 10^0$	$5.88 \times 10^0$
$1.11 \times 10^{-1}$	$2.62 \times 10^{15}$	$4.47 \times 10^{-2}$	$1.04 \times 10^{+1}$	$9.92 \times 10^0$
$1.73 \times 10^{-1}$	$4.27 \times 10^{15}$	$2.87 \times 10^{-2}$	$1.46 \times 10^{+1}$	$1.25 \times 10^{+1}$
$2.22 \times 10^{-1}$	$5.85 \times 10^{15}$	$2.24 \times 10^{-2}$	$1.80 \times 10^{+1}$	$1.41 \times 10^{+1}$
$3.33 \times 10^{-1}$	$8.89 \times 10^{15}$	$1.49 \times 10^{-2}$	$2.37 \times 10^{+1}$	$1.71 \times 10^{+1}$
$5.93 \times 10^{-1}$	$1.82 \times 10^{16}$	$8.38 \times 10^{-3}$	$3.03 \times 10^{+1}$	$2.11 \times 10^{+1}$
$7.84 \times 10^{-1}$	$2.63 \times 10^{16}$	$6.35 \times 10^{-3}$	$3.34 \times 10^{+1}$	$2.47 \times 10^{+1}$
C <sub>2</sub> H <sub>2</sub>				
$P$ (Torr)	$dN/dt$ (s <sup>-1</sup> )	$\lambda$ (cm)	$\theta_{1/2}$ (deg)	$\theta_{1/2}^c$ (deg)
$4.37 \times 10^{-4}$	$1.87 \times 10^{13}$	$6.40 \times 10^0$	$4.05 \times 10^0$	$4.15 \times 10^0$
$5.16 \times 10^{-3}$	$1.19 \times 10^{14}$	$5.42 \times 10^{-1}$	$5.00 \times 10^0$	$4.80 \times 10^0$
$8.73 \times 10^{-3}$	$1.91 \times 10^{14}$	$3.20 \times 10^{-1}$	$5.10 \times 10^0$	$4.50 \times 10^0$
$2.27 \times 10^{-2}$	$5.19 \times 10^{14}$	$1.23 \times 10^{-1}$	$5.60 \times 10^0$	$5.10 \times 10^0$
$3.65 \times 10^{-2}$	$8.11 \times 10^{14}$	$7.65 \times 10^{-2}$	$7.25 \times 10^0$	$6.63 \times 10^0$
$4.37 \times 10^{-2}$	$9.78 \times 10^{14}$	$6.40 \times 10^{-2}$	$8.30 \times 10^0$	$7.90 \times 10^0$
$4.70 \times 10^{-2}$	$1.05 \times 10^{15}$	$5.95 \times 10^{-2}$	$9.50 \times 10^0$	$8.44 \times 10^0$
$5.50 \times 10^{-2}$	$1.19 \times 10^{15}$	$5.09 \times 10^{-2}$	$9.60 \times 10^0$	$9.10 \times 10^0$
$7.27 \times 10^{-2}$	$1.62 \times 10^{15}$	$3.85 \times 10^{-2}$	$1.20 \times 10^{+1}$	$1.00 \times 10^{+1}$
$1.26 \times 10^{-1}$	$3.14 \times 10^{15}$	$2.23 \times 10^{-2}$	$1.65 \times 10^{+1}$	$1.28 \times 10^{+1}$
$1.34 \times 10^{-1}$	$3.20 \times 10^{15}$	$2.09 \times 10^{-2}$	$1.72 \times 10^{+1}$	$1.33 \times 10^{+1}$
$1.59 \times 10^{-1}$	$3.92 \times 10^{15}$	$1.76 \times 10^{-2}$	$2.04 \times 10^{+1}$	$1.55 \times 10^{+1}$
$2.06 \times 10^{-1}$	$5.17 \times 10^{15}$	$1.36 \times 10^{-2}$	$2.35 \times 10^{+1}$	$1.67 \times 10^{+1}$
$2.23 \times 10^{-1}$	$5.70 \times 10^{15}$	$1.26 \times 10^{-2}$	$2.47 \times 10^{+1}$	$1.91 \times 10^{+1}$

After these measurements, we extended the number of degrees of freedom of our detector so that it could also move along  $r$ . Using this, we measured the gas intensity as a function of  $\theta$  for several fixed  $r$  values of 4, 10, 15 and 20 mm.

### 3. Results

#### 3.1. Single-tube data

**3.1.1. Source pressure versus flow rate.** In figures 6(a) and (b), we show the behaviour of  $\dot{N}$  as a function of  $P$ . Fits

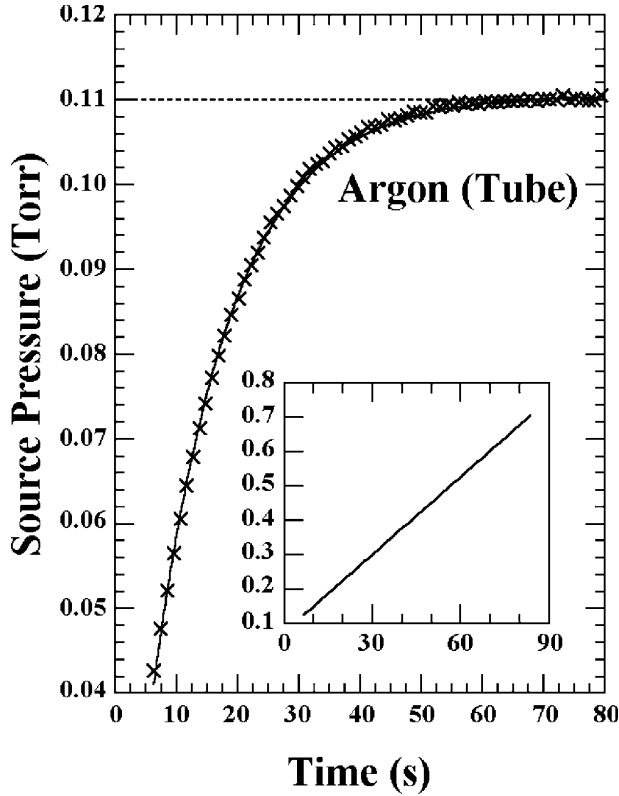


**Figure 4.** Graphs of  $P$  versus  $t$  for the flow of gas through the collimating source, showing the exponential-type behaviour related approximately by equation (5) ( $\times$ , experimental data; and —, fit to experimental data using equation (5)). The inset shows  $dP/dt$  (Torr  $s^{-1}$ ) versus time (s) for all valves except LV in figure 3 closed.

to this using a form from Sagara and Boesten (1998), namely

$$\dot{N} = aP(1 + \varepsilon P) \quad (6)$$

are displayed in table 3. The parameters  $a$  and  $\varepsilon$  are plotted as functions of  $1/\sqrt{M}$  and the gas kinetic cross-section  $\sigma$  ( $= \pi\delta^2$ , where  $\delta$  is the molecular diameter) in figures 7(a) and (b), respectively.

For the range of  $P$  within which  $K_L > 1$  (i.e. inter-atomic/molecular collisions within the tube are negligible) one expects to find a simple linear relation of  $\dot{N}$  to  $P$  with the constant of proportionality,  $a$ , inversely dependent on  $\sqrt{M}$ , where  $M$  is the molar mass number. This relation is well known from the kinetic theory of ideal gases ( $P = nkT$ ). For this case of free-molecular flow without inter-molecular collisions the flow rate (see e.g. Dushman (1949) and Guthrie (1963)) is given by

$$\dot{N} = \kappa \left( \frac{n}{4} A \langle v \rangle \right) = \kappa \left( \frac{(8N_A)^{1/2}}{(\pi MkT)^{1/2}} AP \right)$$

and thus in equation (6)

$$a = \kappa \left( \frac{(8N_A)^{1/2}}{(\pi MkT)^{1/2}} A \right). \quad (7)$$

where  $n$  is the number density behind the source. In equation (7), the mean speed of the gas (Ramsey 1990)

$$\langle v \rangle = \frac{(8kTN_A)^{1/2}}{(\pi M)^{1/2}}. \quad (8)$$

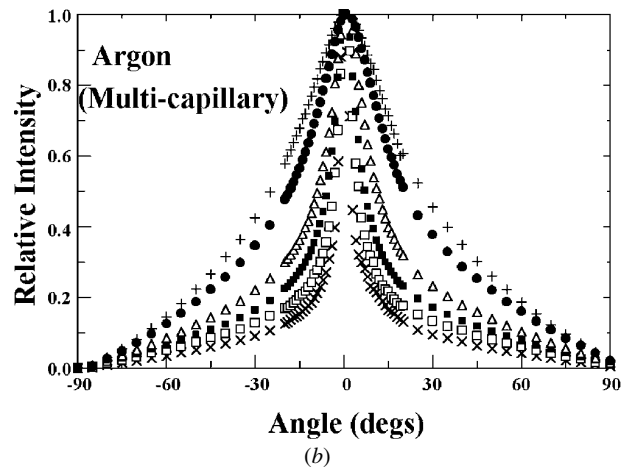
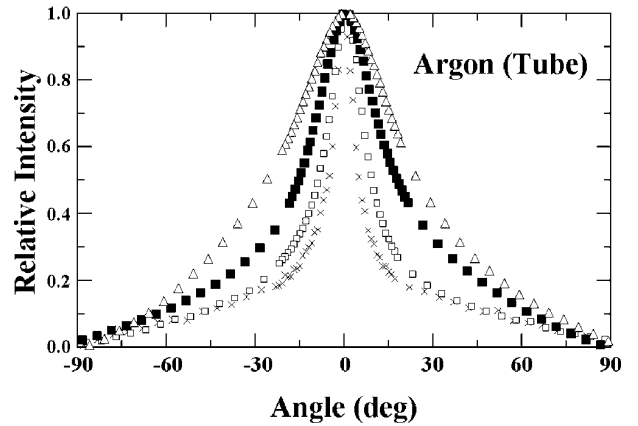


**Figure 5.** (a) A selection of gas beam profiles for our single tube source for various  $P$ , using Ar gas: values of  $P$  are ( $\times$ ), 0.014 Torr; ( $\square$ ) 0.040 Torr; ( $\blacksquare$ ) 0.12 Torr; and ( $\blacktriangle$ ) 0.62 Torr. (b) A selection of gas beam profiles for our multi-capillary tube source for various  $P$ , using Ar gas: values of  $P$  are ( $\times$ ), 0.0085 Torr; ( $\square$ ), 0.092 Torr; ( $\blacksquare$ ), 0.170 Torr; ( $\triangle$ ), 0.400 Torr; ( $\bullet$ ), 1.73 Torr; and (+), 4.95 Torr.

Here we have also used the ideal gas equation  $P = nkT$  in equation (7).  $N_A$  and  $k$  are Avogadro's number and Boltzmann's constant, respectively. The expression in the large parentheses in equation (7) is the well-known law for effusion of atoms out of a thin aperture of area  $A$ ; thus  $\kappa$  is the geometrical transmission (or Clausing factor, see Clausing (1930) and Olander and Kruger (1970)).

The parameter  $\varepsilon$  can be regarded as a first-order deviation from free-molecular flow, i.e. the Knudsen or viscous flow regime. To first order, Knudsen's empirical equation gives the rate of flow through a cylindrical tube (see section 3 and equation (1) of Dushman (1949)) to be of the form

$$\dot{N} = \frac{D}{12L} An \langle v \rangle + \frac{\pi D^4}{2^7 \eta L} n \quad (9)$$

where the Clausing factor  $\kappa = D/(3L)$  is used for a cylindrical tube of length  $L$  and diameter  $D$ . The viscosity  $\eta$  can be obtained from the Chapman–Enskog relations

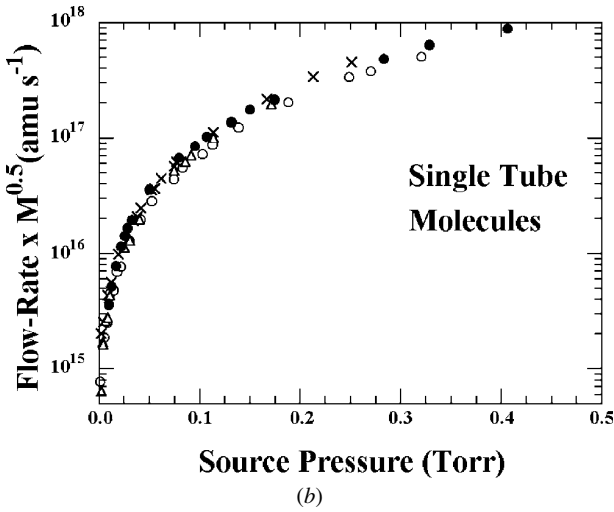
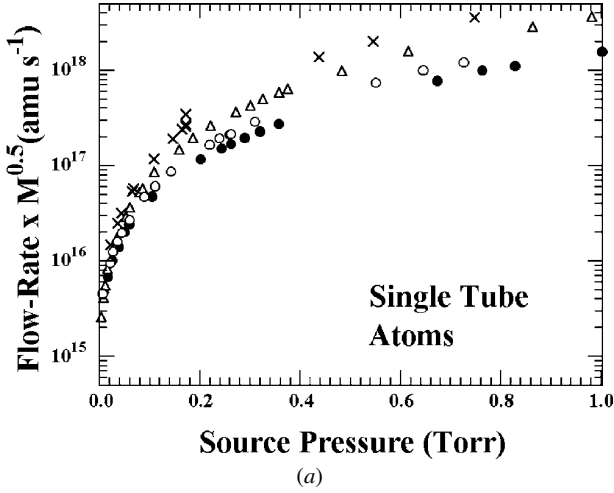


**Figure 6.** (a)  $\sqrt{M} dN/dt$  versus  $P$  plots using the single-tube source for various atomic gases: (●), He; (○), Ne; (△), Ar; and (×), Xe. (b) The same as (a) but for molecules: (●), H<sub>2</sub>; (○), N<sub>2</sub>; (▲), C<sub>2</sub>H<sub>2</sub>; and (×), CO<sub>2</sub>.

(Bird 1994) as

$$\eta = \frac{M}{3N_A} \langle v \rangle \lambda = \frac{5}{16\delta^2} \left( \frac{MkT}{\pi N_A} \right)^{1/2}. \quad (10)$$

$\lambda$  is the mean free-path of the gas and is

$$\lambda = \frac{1}{\sqrt{2\pi n\delta^2}}. \quad (11)$$

Straightforward manipulation of equation (9), using equations (8) and (10), yields

$$\dot{N} = \left( \frac{D\sqrt{N_A}}{3L(2\pi MkT)^{1/2}} A \right) P \left( 1 + \frac{3\sqrt{\pi}\delta^2}{10\sqrt{2kT}} DP \right). \quad (12)$$

which can be written in the more general form

$$\dot{N} = \left( \frac{\sqrt{N_A}}{(2\pi MkT)^{1/2}} A \right) \kappa P (1 + \alpha\delta^2 P). \quad (13)$$

Note that, for a constant  $T$ ,  $\alpha$  is independent of the molecule used. On comparing equations (6) and (13), we see that the

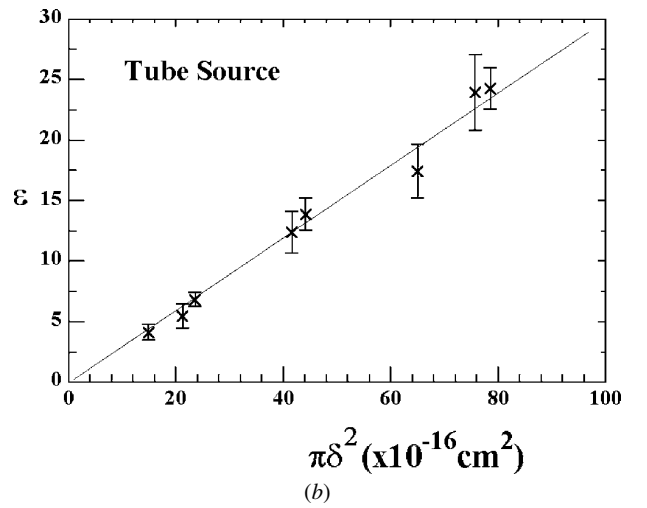
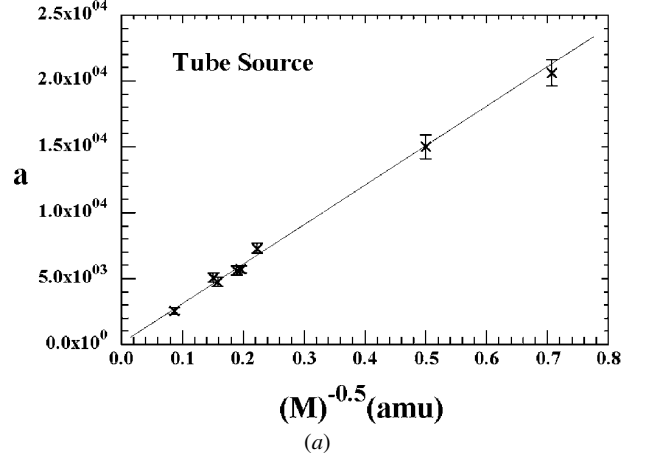
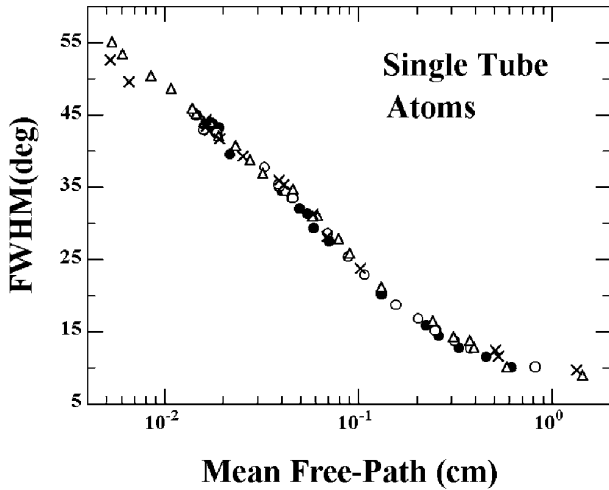


**Figure 7.** (a) The dependence of the parameter  $a$  (equation (6)) on  $1/\sqrt{M}$ , obtained from the single-tube  $dN/dt$  versus  $P$  data. (b) The dependence of the parameter  $\varepsilon$  (equation (6)) on the molecular gas kinetic cross-section ( $\pi\delta^2$ ), obtained from the single-tube  $dN/dt$  versus  $P$  data.

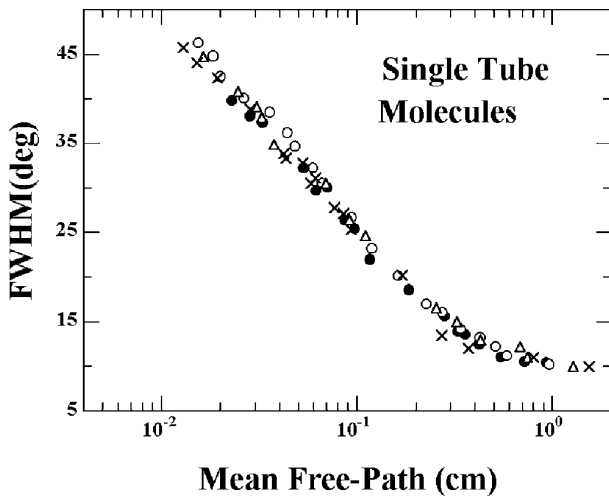
non-linearity parameter  $\varepsilon (= \alpha\delta^2)$  is dependent on  $\delta^2$  of the molecule used.

Using the above equations, in figure 7(a) we observe excellent agreement of the flow rate with  $1/\sqrt{M}$ , which agrees with equation (7) in the free-molecular flow limit. A similar result is observed in figure 7(b) and, by using the first-order flow-rate equation (13), we obtain a normalized ratio of  $\pi\delta^2$  of the gases used in comparison with He ( $\delta = 2.18 \times 10^{-8}$  cm), to estimate their molecular diameters. These normalized molecular diameters,  $\delta_R$ , are given in table 3 and are in good agreement with the existing values of  $\delta$ , within error bars, of around 18%. In figure 7(b), for the normalization and comparisons outlined above, we have used the values of  $\delta$  from Dushman (1949), who gives the most extensive compilation of such values (see also table 2).

**3.1.2. Mean free-path versus angular spread.** From figures 5(a) and 5(b) we note the remarkably large ‘shoulders’ in these gas beam profiles, which are typically observed for  $\theta > 20^\circ$ . These shoulders are very much reduced



(a)

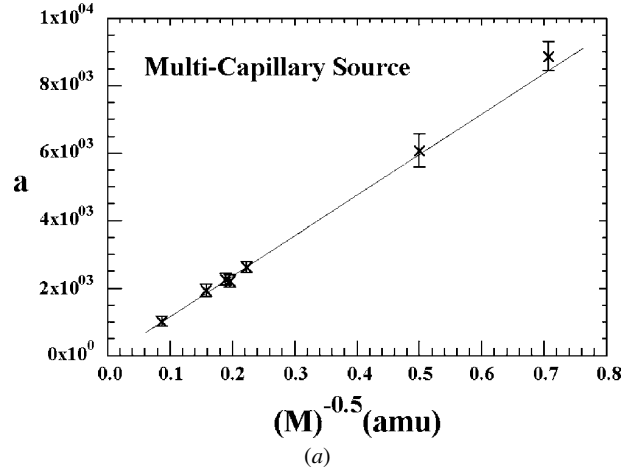


(b)

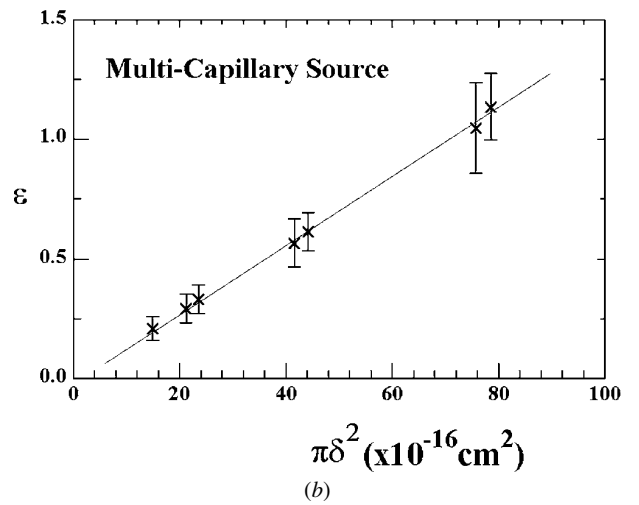
**Figure 8.** (a) Gas beam  $\theta_{1/2}$  values versus  $\lambda$  for atomic gases, using the single-tube source. The symbols have the same meanings as those in figure 6(a). (b) Gas beam  $\theta_{1/2}$  values versus  $\lambda$  for molecular gases, using the single-tube source. The symbols have the same meanings as those in figure 6(b).

in measurements of type B, because the sensitivity of the detector in type B experiments drops as  $\cos^3(\theta)$ . In addition, the profiles are also asymmetrical about  $\theta = 0^\circ$ . This is influenced by the filament's position in the detector. If the filament is placed so that it emits electrons towards the grid in a direction perpendicular to the plane of rotation of the detector, this asymmetry is significantly reduced, since the ionization region is not affected by  $\theta$ .

The FWHM,  $\theta_{1/2}$ , is generally used to quantify a gas beam profile. Such a parameterization of profiles which need not maintain exactly similar shapes is at first debatable. Nevertheless, its relevance to the quantification of gas beams will be discussed in part III, where the whole profile will be considered in the relative-flow calculation. For the case that  $K_L \gg 1$ ,  $\theta_{1/2}$  is expected to be essentially independent of inter-atom/molecule collisions, but should start to increase as these become significant. In this regime Giordmaine and



(a)



(b)

**Figure 9.** (a) The dependence of the parameter  $a$  (equation (6)) on  $1/\sqrt{M}$ , obtained from the multi-capillary source  $dN/dt$  versus  $P$  data. (b) The dependence of the parameter  $\epsilon$  (equation (6)) on the molecular gas kinetic cross-section ( $\pi\delta^2$ ), obtained from the multi-capillary source  $dN/dt$  versus  $P$  data.

Wang (1960) give, for a tube, a simple result, namely

$$\theta_{1/2} = 1.68D/L. \quad (14)$$

For the tube source with a  $D/L$  ratio of 0.04,  $\theta_{1/2}$  in the regime of  $K_L > 1$  (according to equation (12)) is  $\approx 4^\circ$ . Folding this together with our (larger) instrumental angular resolution of  $2^\circ$  FWHM (including the spatial size of the tube) results in a calculated  $\theta_{1/2}$  of  $4.5^\circ$  in the  $K_L > 1$  regime. However, this is not observed in the present work (figures 8(a) and (b)), in which our minimum  $\theta_{1/2}$  is observed to be  $\approx 10^\circ$ . We have compared this  $\theta_{1/2}$  value with other experimental results (Adams and McGilp 1986, 1988) obtained using a source with a similar aspect ratio and find that their experiment also gave significantly larger  $\theta_{1/2}$  than that predicted by equation (14). We also note that, in the present measurements (see figure 8(a)),  $\theta_{1/2}$  is still decreasing and, in the regime of  $K_L \gg 1$ ,  $\theta_{1/2}$  would be difficult to measure because of the reduced fluence of atoms/molecules. In the regime of  $K_D \approx 1$ , the gas beam profile is dominated by collisions in the last  $D$  length of the tube.

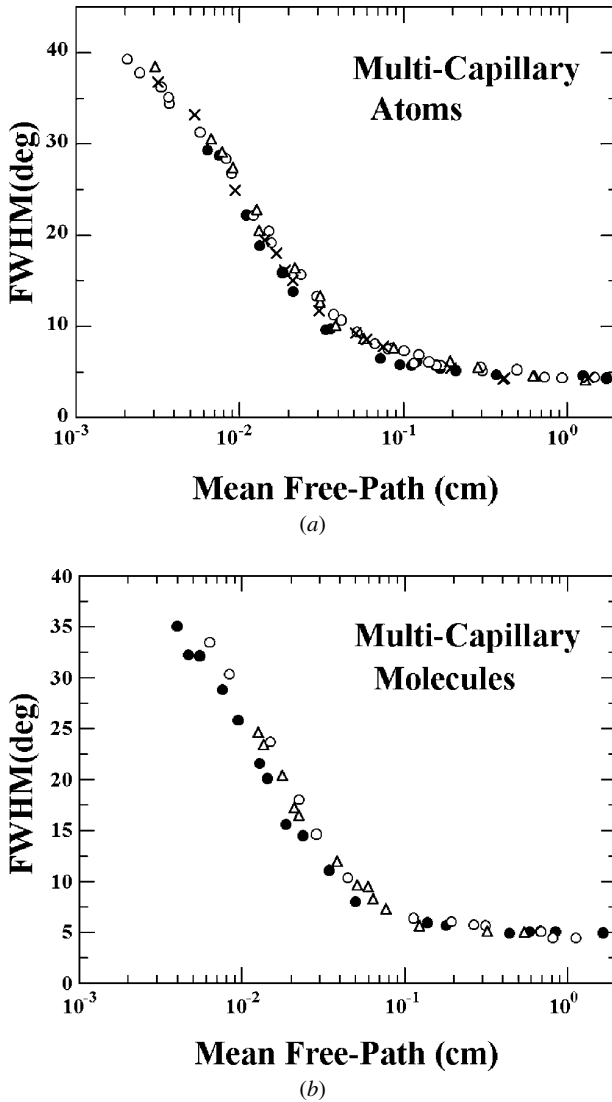


**Figure 10.** (a) Gas beam  $\theta_{1/2}$  values versus  $\lambda$  for atomic gases, using the multi-capillary tube source. The symbols have the same meanings as those in figure 6(a). (b) Gas beam  $\theta_{1/2}$  values versus  $\lambda$  for molecular gases, using the multi-capillary tube source: (●), H<sub>2</sub>; (○), N<sub>2</sub>; and (△) C<sub>2</sub>H<sub>2</sub>.

The gas beam profile is determined by collisions with the tube walls as well as inter-gas collisions. In the limit that inter-gas collisions do not occur ( $\lambda \gg L$ ), it is entirely determined by the geometry of the tube. When inter-atom/molecule collisions occur, the mean free-path becomes an important parameter which controls  $\theta_{1/2}$  (see e.g. Girodmaine and Wang (1960)).

The dependence of  $\theta_{1/2}$  on  $\lambda$  (which was obtained from our gas beam profiles) is plotted for the gases used in figures 8(a) and (b). The values of  $\sigma$  used in our determination of  $\lambda$  were taken from table 2 (present data) and the value of  $n$  is related to the pressure  $P_s$  by the ideal gas equation,  $P = nkT$ .  $\theta_{1/2}^c$  is the gas beam profile  $\theta_{1/2}$  multiplied by  $\cos^3(\theta)$ , to convert type A gas beam profiles into type B profiles.  $\theta_{1/2}$  and  $\theta_{1/2}^c$  are given in table 4 for the case of atoms and in table 5 for molecules.

From figures 8(a) and (b), we observe that  $\lambda$  versus  $\theta_{1/2}$  is essentially independent of the type of gas for a remarkably

large range of pressure. For  $\lambda \geq L$ , we note the weak dependence of  $\theta_{1/2}$  on  $\lambda$ . As  $\lambda$  decreases,  $\theta$  increases, starting from a little above  $\lambda \approx L$  and continuing over a range exceeding  $\lambda < D$ . Closer scrutiny of this  $\theta_{1/2}$  dependence (limited by the accuracy of our data,  $\Delta\theta = \pm 0.75^\circ$ ) for various gases shows that He produced significantly narrower profiles than did any of the other gases across the pressure range studied whereas Xe gave wider beam profiles. This result affirms the observations of Buckman *et al* (1993). However, our variation (e.g. at  $\lambda \approx D = 0.08$  cm mean free-path) is in general smaller, i.e. of the order of 10% of  $\theta_{1/2}$ , than theirs, i.e. of the order of 30% of  $\theta_{1/2}^c$  of He over other gases. Similar conclusions can be drawn concerning  $\theta_{1/2}^c$ . In their measurements, however, Buckman *et al* operated closer to the tube and used a multi-capillary source. However, similar conclusions were drawn with our multi-capillary source data (see section 3.2). Additional measurements (with  $r$  values closer to those of Buckman *et al*) were therefore made, in an attempt to investigate this difference. This fact is addressed further in section 3.3.

### 3.2. Multi-capillary data

**3.2.1. Source pressure versus flow rate.** An analysis similar to that for the single-tube source data was conducted for the multi-capillary source data. We fitted the  $dN/dt$  versus  $P$  measurements to equation (6). The resultant  $a$  and  $\varepsilon$  parameters are plotted against  $1/\sqrt{M}$  and  $\pi\delta^2$  (the molecular collision cross-section), respectively, in figures 9(a) and (b). Again, as in figure 7(a), we observe excellent linearity between  $a$  and  $1/\sqrt{M}$  in figure 9(a). From the linear result in figure 8(b), (see section 3.1.1 for the tube) we can also determine molecular diameters relative to He. However, the uncertainties in these  $\delta$  values are larger than those obtained from the tube results. This is because the second-order term observed (see equation (6)) for the multi-capillary array  $dN/dt$  versus  $P$  data is small relative to the first-order term in comparison with the  $dN/dt$  versus  $P$  data for the single tube. These results are given in table 6. Again, good agreement with available  $\delta$  values (table 2) is found.

**3.2.2. Mean free-path versus angular spread.** Tables 7 and 8 summarize the profiles and flow rates of several atomic and molecular species passing through the capillary array. Figures 10(a) and (b) show the dependence of  $\theta_{1/2}$  on  $\lambda$ . These figures (similarly to figures 8(a) and (b)) again show the strong dependence of the angular spread of the gas beam on the mean free-path. However, it is very clear that He produces significantly narrower beams than do the other gases (narrower by  $>1.5^\circ$  in places), which produce beams of comparable widths. This is similarly followed by the narrow profiles produced by H<sub>2</sub>. This trend agrees with the measurements of Buckman *et al* (1993) but our results show a smaller variation in  $\theta_{1/2}$  than do theirs. Also, this difference between He and H<sub>2</sub> profiles and those of the heavier gases is not as pronounced as that for the tube source. For  $\lambda \approx 0.1$  cm ( $K_D \approx 1$ ), we observe a flat behaviour of  $\theta_{1/2}$  versus  $\lambda$ . In this regime the value of  $\theta_{1/2}$  is  $4.65^\circ \pm 0.75^\circ$ . This does not correspond to the angle subtended by a tube with an aspect ratio of 0.01, which should

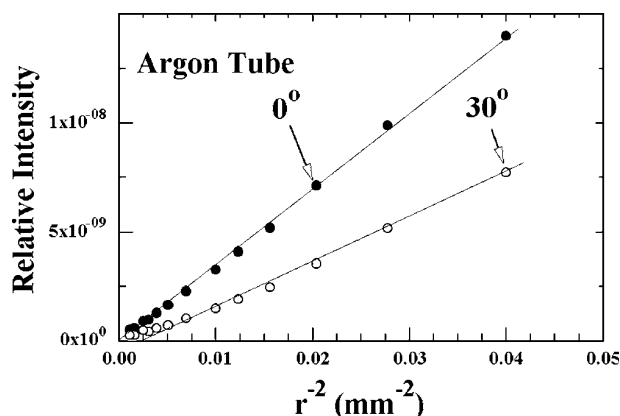


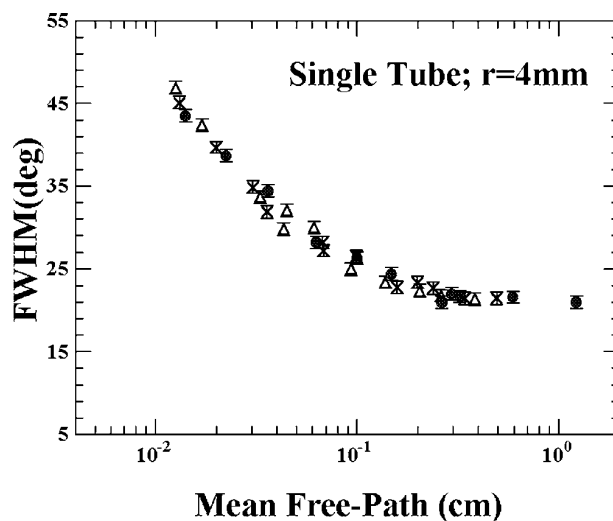
**Figure 11.** The dependence of the relative intensity of the gas beam versus  $1/r^2$  for Ar gas. See the text for a discussion.

be (according to equation (14))  $\approx 1^\circ$ . Folding in our (larger) angular resolution of  $2^\circ$  still leaves an overall profile FWHM of  $2.25^\circ$ . Equation (12) clearly does not explain the larger  $\theta_{1/2}$  measured. This larger  $\theta_{1/2}$  value is also observed in other experiments using multi-capillary sources (Buckman *et al* 1993).

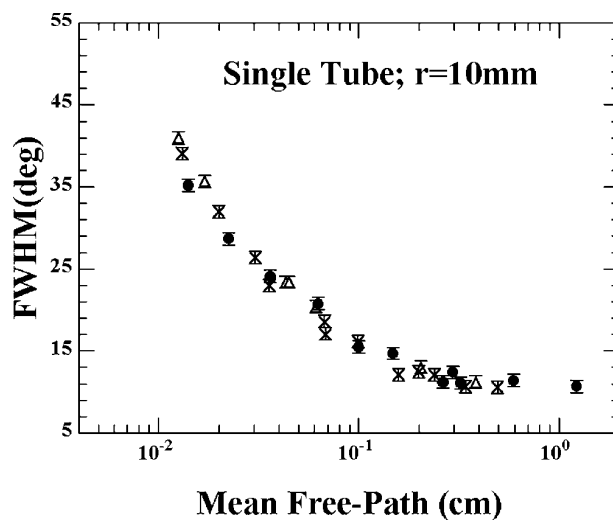
Clearly, a mechanism other than pure specular reflection off the tube walls is needed in order to obtain the geometrical collimation of the atoms/molecules by the tube alone. One could consider e.g. other atom–tube-wall reflection mechanisms, e.g. the slip model considered by Thomson and Owens (1975). Comparison with  $\theta_{1/2}$  versus  $\lambda$  for molecules shows that it exhibits a significantly larger spread than does that for atoms. Whereas for atoms differences in  $\theta_{1/2}$  of  $\approx 10\%$  exist, for molecules (e.g.  $H_2$  versus  $N_2$ ) these differences are as much as 25%. This is in very good agreement with the results of Buckman *et al* (1993); however, their work showed that this disagreement extended to atoms as well, which is not observed here. Additionally, they observed a significantly larger disagreement in  $\theta_{1/2}$  between various gases as  $r$  was increased, which is not observed here.

### 3.3. Three-dimensional measurements

In addition to being able to scan in  $\theta$  at fixed  $r$ , we modified our ion gauge detector in order to be able to vary  $r$  up to 30 mm using an in-vacuum linear motion track coupled to an in-vacuum stepping motor. The ionization gauge detector used in these studies had a nozzle of diameter 0.2 mm. The distance from the exit of the source was monitored with a linear potentiometer that had been calibrated *in situ*. We tested the reliability of our detector by monitoring the ion signal  $I_s$  versus  $r$  using Ar gas. These results are shown in figure 11, in which the relative intensity ( $\propto I_s$ ) is plotted against  $r^{-2}$ . Clearly the inverse-square law applies very well, but there are departures from the straight-line plot as one gets closer to the tube than 1 mm away. This deviation, in part, could be due to the accuracy of our determination of the absolute value of  $r$  in the sub-millimetre regime, an error which greatly affects  $1/r^2$  as one gets closer to the tube. This error was examined by varying  $r$  by  $\pm 0.25$  mm and attempting to fit the intensity versus  $1/r^2$  of figure 11. This procedure failed to account for the deviation at small  $r$ .



(a)



(b)

**Figure 12.** (a) Gas beam  $\theta_{1/2}$  values versus  $\lambda$  for atomic gases, using the single-tube source but taken at  $r = 4$  mm: (●), He; (Δ), Ar; and (×), Xe. (b) The same as (a), but taken at  $r = 20$  mm.

We consequently suspect this deviation to be due to the importance of the spatial extent of the source gas for small  $r$  and, to some extent, to the shape of the gas distribution at the boundary between the tube source and the vacuum and possibly the roughness of the tube at its exit.

We measured gas beam profiles for a group of atoms, i.e. He, Ar and Xe, for  $r$  values of 4, 10, 15 and 20 mm. Plots of  $\theta_{1/2}$  versus  $\lambda$  for the various gases for  $r$  values of 4 and 20 mm are shown in figures 12(a) and (b). We observe a little variation of the beam profiles from the mean free-path dependence. However, when these variations are averaged over the pressure range, they are not significant, even when one is working close to the gas beam. Any variation, e.g. for Ar in figure 12(b), can be accounted for in terms of the uncertainty in the  $\delta$  value of the gas. We thus conclude that (at least for atoms) the mean free-path holds very well in terms of controlling the gas beam profile, for a wide range of source pressures as well as distances from the tube exit. Again we

note that, with our decreased detector angular resolution of  $0.6^\circ$ , we still measure a low pressure limit of  $\theta_{1/2} \approx 7^\circ$  greater than the  $4^\circ$  value of equation (12). Interestingly, we observe that, for  $r \approx 4$  mm, the spatial extent of the source itself brings about a flattening of the gas beam profile around  $\theta = 0^\circ$ . This yields the significantly larger  $\theta_{1/2}$  values displayed in figure 12(a). Nevertheless this does not affect the mean free-path condition, as can be observed in figure 12(a), but shows clearly that the spatial extent of the gas source tube needs to be included in evaluations of such profiles at small  $r$  values.

#### 4. Conclusions

We have presented extensive data for gas beam profiles and flow rate characteristics of gas beams flowing through two collimating tube structures. The flow rate results show that good agreement is obtained by characterizing the pressure dependence of the flow in terms of a quadratic expression (equation (6)) in the first-order non-linear region. This also gives very good agreement with existing models of flow in the viscous (Knudsen) region and with the recent modelling of Sagara and Boesten (1998). From these models (described in Dushman (1949)), we were able to obtain relative molecular diameters which were normalized with respect to that of He.

We observe good adherence of the mean free-path dependence of  $\theta_{1/2}$  and  $\theta_{1/2}^c$  for all the moderately heavy gases. Significant variation is observed for He and H<sub>2</sub> versus the heavier gases, but it is found that the difference in gas beam profiles is larger for the multi-capillary source than it is for the tube. Our measurements differ from the results of Buckman *et al* (1993) in that, despite our reasonable angular resolution, we fail to see large deviations from the mean free-path characterization of the gas beam profile for atomic species. We also observe the significance of shoulders in the angular profiles, for  $\theta > 20^\circ$ .

In an effort to understand how these shoulders are produced and how the sharpness of the forward distribution is affected by collisions, we have developed a Monte Carlo simulation of the flow conditions in the tubes which includes the consideration of flow rates. The Monte Carlo simulations, for example, clearly indicate that these shoulders are predominantly determined by wall collisions in the last diameter of the tube length. In addition, they show how small angle inter-gas scattering enhances the forward profile, whereas large angle scattering reduces the forward profile. These results will be detailed in part II and compared with existing analytical models.

The above results can be used to obtain some practical knowledge concerning the application of the relative flow

method (Srivastava *et al* 1975, Trajmar and Register 1984) and the systematic measurement of gas beam profiles. In part III we will use the present gas profiles' data to investigate the sensitivity of the relative flow method to variations in gas beam parameters.

#### Acknowledgments

This project was funded by a California State University mini-grant and by the National Science Foundation of the USA (grant NSF-RUI-PHY-9511549). MAK would like to thank Dr Timothy J Gay (University of Nebraska, Lincoln) for helpful discussions. Expert technical help from David Parsons (in the CSUF machine shop) and Hugo Fabris (in the CSUF electronic shop) are also acknowledged. M Rudner and J Shih were involved in this research as Troy High School senior students under the Troy Tech programme.

#### References

- Adamson S and McGilp J F 1988 *Vacuum* **36** 227
- 1988 *Vacuum* **38** 463
- Adamson S, O'Carroll C and McGilp J F 1988 *Vacuum* **38** 341
- Bird G A 1994 *Molecular Gas Dynamics and the Direct Simulation of Gas Flows* (Oxford: Oxford University Press)
- Brinkmann R T and Trajmar S 1981 *J. Phys. E: Sci. Instrum.* **14** 245
- Buckman S J, Gulley R J, Moghbelalhossein M and Bennett S J 1993 *Meas. Sci. Technol.* **4** 1143
- Clausing P 1930 *Z. Phys.* **66** 471
- 1969 *CRC Handbook* 5th edn (Boca Raton, FL: CRC) F151
- Dushman S 1949 *Vacuum Technique* (New York: Wiley) pp 36 and 43
- Giordmaine J A and Wang T C 1960 *J. Appl. Phys.* **31** 463
- Guthrie A 1963 *Vacuum Technology* (New York: Wiley) p 504
- Hanes G R 1960 *J. Appl. Phys.* **31** 2171
- Jones R H, Olander D R and Kruger V R 1969 *J. Appl. Phys.* **40** 4641
- Khakoo M A, Jayaweera T, Wang S and Trajmar S 1993 *J. Phys. B: At. Mol. Opt. Phys.* **26** 4845
- Lucas C B 1973 *Vacuum* **23** 395
- Murphy D M 1989 *J. Vac. Sci. Technol. A* **7** 3075
- Olander D R and Kruger V R 1970 *J. Appl. Phys.* **41** 4641
- Ramsey N F 1990 *Molecular Beams* 2nd edn (Oxford: Oxford University Press) ch 2
- Roth A 1987 *Vacuum Technology* (New York: Elsevier)
- Sagara T and Boesten L 1998 *J. Phys. B: At. Mol. Opt. Phys.* **31** 3455
- Srivastava S K, Chutjian A and Trajmar S 1975 *J. Chem. Phys.* **63** 2659
- Steinruck H P and Rendulic K D 1986 *Vacuum* **36** 213
- Thomson S L and Owens W R 1975 *Vacuum* **25** 151
- Trajmar S and Register D F 1984 *Electron-Molecule Collisions* ed I Shimamura and K Takayanagi (New York: Plenum) ch 6, p 468
- Trajmar S, Register D F and Chutjian A 1983 *Phys. Rep.* **97** 219
- Zugenmaier P 1965 *Z. Angew. Phys.* **20** 184